DIFFUSION IN NEAR-INTEGRABLE HAMILTONIAN SYSTEMS WITH THREE DEGREES OF FREEDOM

by

J. L. Tennyson, M. A. Lieberman and A. J. Lichtenberg

Memorandum No. UCB/ERL M79/19

5 March 1979

ELECTRONICS RESEARCH LABORATORY

College of Engineering
University of California, Berkeley
94720

DIFFUSION IN NEAR-INTEGRABLE HAMILTONIAN SYSTEMS WITH THREE DEGREES OF FREEDOM

by

J. L. Tennyson, M. A. Lieberman and A. J. Lichtenberg

Department of Electrical Engineering and Computer Sciences

&

The Electronics Research Laboratory

University of California

Berkeley, California 94720

ABSTRACT

We review, using a few simple examples, the mechanism for a very general stochastic motion — the Arnold diffusion — which occurs in near-integrable Hamiltonian systems with more than two degrees of freedom. The examples chosen describe the effect of periodic perturbations on a free particle system in three dimensions. The calculated Arnold diffusion rates are in good agreement with the results of simulation studies.

I. INTRODUCTION

One hundred and forty five years after W. R. Hamilton formulated his famous equations, the long term motion they describe is still not completely understood. The nature of the motion is firstly determined by the degree of symmetry of the Hamiltonian system according to the rule[1] that "the less symmetrical the Hamiltonian system, the more intricate is the motion." For each symmetry, there exists an independent global invariant of the motion. Symmetries may be "visible" or "hidden", and often it is not easy to guess whether or not they exist. A notable example is the Toda lattice Hamiltonian,[2] which apart from the energy has one "visible" and one "hidden" symmetry. There is no known analytic procedure for obtaining the global invariants of the motion for a given Hamiltonian, or even for determining their total number. As stated in a recent review[1], "a theory that could be used to test the presence of one symmetry or another of a given Hamiltonian, and in particular to calculate its degree of symmetry, is still waiting to grow out of 'alchemy' into 'chemistry'. Therefore, eschewing alchemy, we pass this problem by in silence."

In the discussion that follows, we consider only Hamiltonians that are autonomous (the quantity represented by the Hamiltonian function is conserved). Any Hamiltonian that is not autonomous may be made so by introducing an extended phase space.[3]

There are two distinct classes of Hamiltonians, integrable and nonintegrable. For integrable Hamiltonians with N degrees of freedom, N independent symmetries exist (including energy). These

allow for the isolation and independent solution of the motion in each degree of freedom. All trajectories are regular and are confined to an N dimensional surface in the phase space. According to a theorem of Siegal's[4], such Hamiltonians are rare. In the generic case, the Hamiltonian is not completely integrable. Hamiltonians in this second class have M (less than N) independent symmetries. These symmetries may be used to reduce the Hamiltonian to a system with (N-M+1) degrees of freedom which has no global invariants and always displays some stochastic motion. It has been shown[5,6] that in general, these non-integrable Hamiltonians generate a finite proportion of trajectories which are stochastic, and a finite proportion which are integrable. The integrable trajectories do not reflect global invariants of the system since their existence depends discontinuously on the initial conditions. Stochastic and integrable trajectories are intimately commingled, with a stochastic trajectory lying arbitrarily close to every point in the phase space.

For two degrees of freedom, stochastic trajectories may be isolated from one another by integrable (KAM) surfaces. For three degrees of freedom (with only one global invariant), the integrable trajectories still exist, but do not isolate the stochastic trajectories. All stochastic regions of the phase space are connected into a single complex network — the Arnold web. The web permeates the entire phase space, intersecting or lying infinitesimally close to every point. For an initial condition on the web, the subsequent stochastic motion will eventually intersect every finite region of the phase space (or energy surface, for an autonomous system) — this is

the Arnold diffusion.[7,8]

Although the merging of stochastic trajectories into a single web seems to be a general characteristic of $N > 2$ non-integrable systems, there is some controversy, and the question is not entirely settled. Contopoulos *et al.*[9] have performed simulation studies on a particular model with $N = 3$, and have found results which they interpret to indicate the existence of segregated stochastic regions. One of these regions exhibits the usual single invariant (energy), while the others seem to be characterized by a second invariant in addition to the energy. Whether this additional invariant is truly a constant, or whether the slow rate of Arnold diffusion has caused it to appear as a constant, is not yet known.

II. FREE PARTICLE HAMILTONIAN SYSTEMS

We consider Hamiltonians comprised of an integrable part, $H_N^{(0)}$, and a small perturbation, $\varepsilon H_N^{(1)}$,

$$H_N = H_N^{(0)}(\underline{I}) + \varepsilon H_N^{(1)}(\underline{I},\underline{\theta})$$

where $\underline{I}$ and $\underline{\theta}$ are the N-dimensional action and angle vectors of $H_N^{(0)}$, and $H_N^{(1)}$ is periodic in $\underline{\theta}$ with period 2π. The stochastic web appears in the neighborhood of the resonances of the unperturbed Hamiltonian. The resonances are the closed, periodic trajectories of $H_N^{(0)}$.

As a specific example, we examine in detail the system shown in Fig. 1. A free particle moving in three dimensions is subject

to the influence of a small, spatially periodic perturbation,

$$H = \frac{p^2}{2m} + \varepsilon \sum_{\underline{m}} V_{\underline{m}} e^{i\underline{m}\cdot\underline{\theta}} + \text{c.c.} \tag{1}$$

where $\underline{m}$ is called the resonance vector and has three integer components. We also have

$$\theta_j \equiv K_j x_j$$

$$K_j \equiv \frac{2\pi}{\lambda_j} .$$

For simplicity, we assume the components of $\underline{K}$ to be equal, $K_j = K$. The case of unequal K_j differs trivially from the one considered here.

The action-angle variables for the unperturbed motion are

$$\underline{I} \equiv \frac{m}{K} \underline{v} \tag{2}$$

$$\underline{\theta} \equiv K \underline{x} \tag{3}$$

$$\underline{\omega}(\underline{I}) \equiv \frac{K^2}{m} \underline{I} . \tag{4}$$

Note that the system is nonlinear in the sense that $\underline{\omega}$ is proportional to $\underline{I}$ (and also to $\underline{v}$). The Hamiltonian in the new variables is

$$H = \tfrac{1}{2} \frac{K^2}{m} I^2 + \varepsilon \sum_{\underline{m}} V_{\underline{m}} e^{i\underline{m}\cdot\underline{\theta}} + \text{c.c.} . \tag{5}$$

When $\varepsilon = 0$, the projection of the motion into the three dimensional frequency space (which is also the action and velocity spaces) is a single point which may or may not represent a resonance. The set of resonance frequencies is defined by

$$\underline{m}\cdot\underline{\omega} = 0 \qquad \text{(for all } \underline{m}\text{)} .$$

Thus, for a given $\underline{m}$, the loci of resonance points lie in a resonance plane which is perpendicular to $\underline{m}$ and passes through the origin. The resonance vectors $\underline{m}$ are shown in Fig. 2 (for $m_i = -2,-1,0,+1,+2$). The resonance planes are perpendicular to these vectors and the entire set intersects every finite region of the action space. The intersection of the resonance planes with the unperturbed energy surface

$$I_1^2 + I_2^2 + I_3^2 = \text{constant}$$

is shown in Fig. 3. The intersection forms a network of resonance lines called the "Arnold web". These lines form an everywhere dense set on the energy surface.

We are now in a position to examine the effect of a finite perturbation on the unperturbed motion. We look at three cases in which the perturbation potential has one, two, and three Fourier components, respectively.

We consider first a potential with a single Fourier component $\underline{n}$ (for $V_{\underline{n}}$ independent of $\underline{I}$, this might represent an electrostatic plane wave). Leaving the c.c. notation as understood, the Hamiltonian can be written

$$H = \tfrac{1}{2}\underline{I} \cdot \underline{\omega} + \varepsilon V_{\underline{n}} e^{i\underline{n}\cdot\underline{\theta}} \tag{7}$$

and

$$-\frac{d\underline{I}}{dt} = \frac{\partial H}{\partial \underline{\theta}} = i\underline{n}\varepsilon V_{\underline{n}} e^{i\underline{n}\cdot\underline{\theta}} \ . \tag{8}$$

Thus, the change in the action must always lie in the direction of the resonance vector $\underline{n}$, as shown in Fig. 4. The motion is completely integrable, but the energy surface is thickened by $2\varepsilon V_{\underline{n}}$ and a separatrix forms about the resonance. The phase space trajectories are those of a simple pendulum. Typical libration, rotation, and separatrix motion is shown in Fig. 5. We note that since the motion is always perpendicular to the resonance line, any displacement along the resonance line is forbidden.

Consider now the case of two nonparallel, nonperpendicular Fourier components (two waves),

$$H = \frac{K^2}{2m}\underline{I} \cdot \underline{I} + \varepsilon V_{\underline{n}} e^{i\underline{n}\cdot\underline{\theta}} + \varepsilon V_{\underline{\ell}} e^{i\underline{\ell}\cdot\underline{\theta}} \tag{9}$$

$$i\frac{d\underline{I}}{dt} = \underline{n}\varepsilon V_{\underline{n}} e^{i\underline{n}\cdot\underline{\theta}} + \underline{\ell}\varepsilon V_{\underline{\ell}} e^{i\underline{\ell}\cdot\underline{\theta}} \tag{10}$$

$$\frac{d\underline{\theta}}{dt} = \frac{K^2}{m}\underline{I} + \varepsilon\frac{\partial V_{\underline{n}}}{\partial \underline{I}} e^{i\underline{n}\cdot\underline{\theta}} + \varepsilon\frac{\partial V_{\underline{\ell}}}{\partial \underline{I}} e^{i\underline{\ell}\cdot\underline{\theta}} \ . \tag{11}$$

The two primary resonance lines are shown as heavy curves in Fig. 6. In addition to the primary resonances, the nonlinearity of the motion excites an infinite set of secondary resonances. This can be seen by iteratively solving Eqs. (10) and (11) for $\underline{I}$ and $\underline{\theta}$. We choose

the special case where the $V_{\underline{m}}$ are not functions of $\underline{I}$ (though the results are similar if we include this dependence). Approximating $\underline{\theta} = \underline{\omega} t$ and integrating Eq. (10), we generate the primary resonances

$$\underline{I}(t) \sim A\, \underline{n} \cos(\underline{n} \cdot \underline{\omega} t) + B\, \underline{\ell} \cos(\underline{\ell} \cdot \underline{\omega} t) \quad . \tag{12}$$

Using this result in Eq. (11) and integrating yields

$$\underline{\theta}(t) \sim C\, \underline{n} \cos(\underline{n} \cdot \underline{\omega} t) + D\, \underline{\ell} \cos(\underline{\ell} \cdot \underline{\omega} t) \tag{13}$$

where A,B,C, & D are constants. Using Eq. (13), a second iteration of Eq. (10) now generates an infinite set of second order resonances. For example, in Eq. (10) the term $\underline{n} \exp[i(\underline{n} \cdot \underline{\theta})]$ results in an infinite set of harmonics through the expansion

$$\exp[i\underline{n} \cdot \underline{\theta}] \sim \sum_{m_1 m_2} J_{m_1}(C)\, J_{m_2}(D\underline{n} \cdot \underline{\ell}) \exp[i(m_1\, \underline{n} + m_2\, \underline{\ell}) \cdot \underline{\omega} t]$$

where the J's are Bessel functions. As can be seen from Eq. (14), all secondary resonances have the form

$$(m_1 \underline{n} + m_2 \underline{\ell}) \cdot \underline{\omega} = 0$$

so the secondary resonance vectors also lie in the $\underline{\ell}$-$\underline{n}$ plane. These are shown as thin lines in Fig. (6).

For small perturbations, thin stochastic layers are formed about each resonance line. The formation of stochastic layers occurs when the separatrices of neighboring secondary resonances overlap.[8] Although the motion is now stochastic near a resonance, the system is

still confined to a small region of the energy surface. As shown by Eq. (10) (and as illustrated by Fig. 7), all trajectories are restricted to planes parallel to the $\underline{\ell}$-$\underline{n}$ plane. Motion along a resonance line (the Arnold diffusion) is not allowed. Note that for a small enough total energy (or a large enough perturbation) the secondary stochastic layers may overlap, leading to diffusion around the intersection of the $\underline{n}$-$\underline{\ell}$ plane and the energy surface. The two wave problem can easily be reduced to two degrees of freedom by separating out the motion in the direction perpendicular to the $\underline{\ell}$-$\underline{n}$ plane.

In our final example, the free particle interacts with three noncoplanar, nonperpendicular Fourier components (or waves). We have

$$\frac{d\underline{I}}{dt} = \underline{n}\,\varepsilon\, V_{\underline{n}} e^{i\underline{n}\cdot\underline{\theta}} + \underline{\ell}\,\varepsilon\, V_{\underline{\ell}} e^{i\underline{\ell}\cdot\underline{\theta}} + \underline{p}\,\varepsilon\, V_{\underline{p}} e^{i\underline{p}\cdot\underline{\theta}} \,. \qquad (15)$$

The three primary resonance lines are shown in Fig. 8. As before, the nonlinearity of the motion generates a web of second order resonances, with

$$(m_1\underline{\ell} + m_2\underline{n} + m_3\underline{p})\cdot\underline{\omega} = 0 \,. \qquad (16)$$

The system may now move in any direction along the energy surface in $\underline{I}$ space. Again, thin stochastic layers form near each resonance line. In contrast to the previous examples, stochastic trajectories may now exhibit Arnold diffusion, moving along the resonance lines and exploring every finite region of the energy surface.

From a practical point of view, there are two major questions concerning Arnold diffusion in a particular system:

(a) What is the relative measure of stochastic trajectories in the phase space region of interest?

(b) How fast will the system diffuse along the thin threads of the Arnold web?

III. THE BILLIARDS PROBLEM

We have studied in detail the motion of a simple physical system with three degrees of freedom. As shown in Fig. 9, a point particle bounces back and forth between a smooth wall located at $z = h$ and a periodically rippled wall located at $z = 0$. The ripple is defined by the equation

$$z = - a_x \cos k_x x - a_y \cos k_y y \qquad (17)$$

which is just a superposition of two perpendicular waves. This "hard wall" system is very similar to the free particle model with a perturbation containing more than three noncoplanar Fourier components. It exhibits both the stable KAM trajectories and Arnold diffusion.

It is possible to describe the motion of the particle in terms of four difference equations. These give the evolution of the trajectory angles (α_n, β_n) and position (x_n, y_n) as defined just before the n^{th} bounce. The system is illustrated in Fig. 10 for $a_y = 0$. In this case the y motion is independent of the x-z motion and the system reduces to two dimensions (stochasticity but no diffusion).

The exact difference equations for this system cannot be written in explicit form, so it is of practical interest (both for analytic

calculations and computational speed) to make some simplifying approximations.

If we assume both

$$|\alpha|, |\beta| \ll \frac{\pi}{2} \qquad \text{and} \qquad a_x k_x, a_y k_y \ll 1$$

the rippled wall may be replaced by a flat wall at $z = 0$ whose normal vector is a function of x and y (this is somewhat analogous to the idea of a Fresnel mirror). The simplified difference equations exhibit most of the general features of the exact equations and may be written in explicit form

$$\alpha_{n+1} = \alpha_n + 2\,\gamma_x\,(x_n, y_n) \tag{18}$$

$$x_{n+1} = x_n + 2\,h\,\tan\,(\alpha_{n+1}) \tag{19}$$

$$\beta_{n+1} = \beta_n + 2\gamma_y\,(x_n, y_n) \tag{20}$$

$$y_{n+1} = y_n + 2h\,\tan\,(\beta_{n+1})\ . \tag{21}$$

These equations may be interpreted as a mapping on the Poincaré surface of section at $z = 0$. A similar set of equations has been studied via computer simulations by Froeschlé and Scheidecker[10].

If γ_x is not a function of y , and γ_y is not a function of x , the system breaks into two uncoupled parts describing motion in x-z and y-z separately. Fig. 11 shows the motion in the α-x surface of section for the uncoupled case. A number of different

trajectories are shown, each with different initial conditions. Each particle was allowed to run for 1000 iterations. The plot displays the usual features of a system with two degrees of freedom. a) stable trajectories b) stochastic trajectories, and c) resonance islands. Of concern for the calculation of diffusion rates are the thick stochastic layers for $|\alpha| \gtrsim (.6)\pi/2$ and the thin stochastic layer that covers the separatrix of the central primary resonance.

Surface of section trajectories have also been computed for the exact problem (a real rippled wall). The motion in the α-x plane is shown in Fig. 12 for the same parameters and initial conditions used in Fig. 11. The basic features of the exact problem are apparently well represented by the approximate equations.

The difference equations, Eqs. (18) - (21), will be truly three dimensional when γ_x includes a dependence on y and γ_y a dependence on x. This can be accomplished by adding a small diagonal ripple to the bottom wall. The (virtual) normal to the surface $z = 0$ at (x,y) is then described by the angles

$$\gamma_x = a_x k_x \sin k_x x + \varepsilon k_x \gamma_c \tag{22}$$

$$\gamma_y = a_y k_y \sin k_y y + \varepsilon k_y \gamma_c \tag{23}$$

where

$$\gamma_c = \sin (k_x x + k_y y) \ . \tag{24}$$

The parameter ε is the amplitude of the diagonal ripple and indicates the magnitude of the coupling between the x motion and the y motion.

As in the case of two degrees of freedom, there are both integrable and nonintegrable trajectories. Unlike the previous case, however, stochastic trajectories are not confined to a particular locality in the phase space.

An example of integrable motion is shown in Fig. 13. Three invariants of the motion exist. The motion is confined to a two dimensional surface in the four dimensional surface of section. The projection of this motion onto the α-x plane yields an annulus of finite area. Figs. 13a and 13b show the motion of a single particle after 5,000 and 50,000 iterations, respectively. The initial conditions were chosen close to the center of the primary resonance. For these intial conditions, the fraction of the phase space area occupied by the Arnold web is very small. It is therefore highly likely, but not absolutely certain, that the motion shown in Fig. 13 is truly integrable. (Computer roundoff errors may destroy this integrability on a very slow time scale.)

We turn, finally, to the featured topic of this paper, stochastic motion in the Arnold web. The stochastic motion for the coupled equations, Eqs. (18) - (24), is characterized by only one (global) invariant. It fills a four dimensional volume in the four dimensional surface of section, and diffuses slowly along the thin stochastic layers which comprise the threads of the pervasive Arnold web. The web itself is composed of an intricate system of "freeways, streets, sidewalks, cracks, etc." that permeates the entire phase space. Particles diffusing along these thin stochastic pathways are able to leave (and penetrate) even the predominantly stable regions of the phase space, where the proportion of stochastic initial conditions is small.

IV. DIFFUSION CALCULATIONS AND SIMULATION RESULTS

We examine two of the diffusion processes that characterize the simplified system, Eq. (18) - (24). The first describes the diffusion of α along the thick stochastic layer of the β-y motion. The quantity α experiences diffusive fluctuations that result from the small coupling to the random y motion. The second process is similar to the first, except that α now diffuses along the thin separatrix layer of the β-y motion. Thick layer diffusion tends to be much faster than thin layer diffusion due to the greater randomness of the y motion in the former case.

In order to calculate the diffusion rates, we adopt a simple model of the diffusion process. For both the "thin" and "thick" layer processes, we assume that the y motion is confined to the stochastic layer. It then acts as a stochastic pump, transporting energy back and forth between the x and z motions. Its own energy may not change except for the small fluctuations necessary to affect the pumping action. (Note that this is not strictly true. It is possible for the system to leave the main resonance along a thin "alleyway", but this turns out to be very unlikely.)

The first step in the calculation is to find a Hamiltonian that will generate the surface of section mappings, Eqs. (18) - (24). In deference to our original model in Fig. 9, we choose a "kicked" Hamiltonian

$$H(\alpha,x,\beta,y,n) = 2h\ \ell n\ [\sec\alpha] + 2h\ \ell n\ [\sec\beta] - 2\delta_1(n)\ C(x,y) \qquad (25)$$

where

$$C(x,y) \equiv a_x \cos k_x x + a_y \cos k_y y + \varepsilon \cos (k_x x + k_y y) \qquad (26)$$

and

$$\delta_1(n) \equiv \sum_{m=-\infty}^{+\infty} \delta(n-m)$$

$$= 1 + 2 \sum_{q=1}^{\infty} \cos (2\pi n q) \ . \qquad (27)$$

Equations (18) - (24) may be derived from Eq. (25) by a simple integration of Hamilton's equations. Note that H in Eq. (25) is a nonautonomous Hamiltonian in two degrees of freedom. It is related to the net energy in the x and y motion, and is not conserved.

For a small enough coupling ε the diffusion is limited by the rate at which energy can be passed back and forth between the x and y motion. Therefore we neglect the explicit coupling to the z motion and take only the $q = 0$ term in Eq. (27). (The z coupling is recognized implicitly in the random phase assumptions that are used later.) This approximation makes Eq. (25) autonomous

$$H(\alpha,x,\beta,y) = 2h\, \ell n\, [\sec \alpha\,] + 2h\, \ell n\, [\sec \beta\,] - 2\, C(x,y) \ . \qquad (28)$$

If we assume α to be small we may simplify the first term

$$\ell n\, [\sec \alpha\,] \sim \frac{\alpha^2}{2} \qquad (29)$$

Equation (28) may be directly reduced to a nonautonomous Hamiltonian for the x motion only

$$H_x = h\alpha^2 - 2a_x \cos k_x x - 2\varepsilon \cos [k_x x + k_y y(n)] , \qquad (30)$$

where y is now considered to be an explicit function of n. Defining $\theta \equiv k_x x$, $\phi(n) \equiv k_y y(n)$ and $\mu \equiv -2\varepsilon$ we have

$$H_x = h\alpha^2 - 2a_x \cos \theta + \mu \cos [\theta + \phi(n)]. \qquad (31)$$

The type of diffusion observed depends upon the initial conditions. For thick layer diffusion, the initial conditions are chosen close to the center of the primary resonance in the α-x plane, and within the thick stochastic layer of the β-y plane. In the absence of coupling $\varepsilon = 0$ the motion in the α-x plane is confined to a smooth closed curve (like those seen close to the center of Fig. 11). The number of bounces required to go exactly once around the curve is the α-period T_α. For a finite coupling, H_x diffuses slowly due to the small randomizing influence of the stochastic β-y motion. The diffusion of H_x is shown in Fig. 14 for 2,000, 10,000, and 30,000 iterations. The motion eventually explores all of the α-x plane. The corresponding motion in the β-y plane is restricted to the thick stochastic layer, at least until the α-x motion reaches its own thick layer.

The diffusion coefficient D_1 for thick layer diffusion has been calculated from Eq. (31), under the assumption that the n dependent variable $\phi(n)$ makes a sudden random jump to a new value whenever n = integer .

The evolution of H_x, from Eq. (31), is

$$\frac{dH_x}{dn} = \frac{\partial H_x}{\partial n} = \mu \sin [\theta + \phi(n)] \frac{d\phi}{dn} \tag{32}$$

$$= \frac{d}{dn} [\mu \cos (\theta + \phi)] - \mu \frac{d\theta}{dn} \sin [\theta + \phi(n)] . \tag{33}$$

The first term contributes only a small oscillation with no net change over long periods of time. For small amplitude libration in the x-α plane, we have

$$\theta \sim \theta_o \cos \omega_o n \tag{34}$$

where

$$\omega_o = \frac{2\pi}{T_\alpha} = 2 k_x (a_x h)^{\frac{1}{2}}$$

Using this, we integrate the second term in Eq. (33)

$$\Delta H_x = \int_m^{m+1} dn \, \mu \, \theta_o \, \omega_o \sin (\omega_o n) \sin [\theta + \phi(n)] . \tag{35}$$

For $\omega_o \ll 1$, this is

$$\Delta H_x \sim \mu \, \theta_o \, \omega_o \sin (\omega_o m) \sin [\theta + \phi(m)] . \tag{36}$$

We square this and average over both m and ϕ to get

$$\langle \Delta H_x^2 \rangle_{t,\phi} = \frac{1}{4} \mu^2 \theta_o^2 \omega_o^2 \tag{37}$$

where we have used the assumption that ϕ is randomized at $m = \text{integer}$. The thick layer diffusion rate is then

$$D_1 = \frac{1}{2} \langle \Delta H^2 \rangle_{t,\phi} = \frac{1}{8} \mu^2 \theta_o^2 \omega_o^2 . \qquad (38)$$

The parameters μ and ω_o will remain fairly constant as H_x diffuses. The quantity θ_o, however, increases with H_x, resulting in an increase in the diffusion rate as the x oscillations grow.

In Fig. 15, the theoretical value of D_1 is compared with measurements obtained from the direct iteration of the difference equations. For each experiment, 100 particles were started with identical initial conditions on a libration curve of the α-x plane, and with random initial conditions in the thick stochastic layer of the β-y plane. The motion was followed for 500 collisions, and the RMS value of the energy $h(\alpha^2)_{RMS}$ was calculated and compared with the theory. Figure 15a shows the variation with coupling strength ε, Fig. 15b the variation with α period T_α, and Fig. 15c the variation with the number of iterations n. The solid lines show the theoretical predictions and the triangles the experimental measurements. Each triangle represents the average of four separate runs. The theoretical predictions, although consistently a little high, are quite good. The discrepancy probably reflects an expected small deviation from true random phase.

We turn now to the thin layer diffusion. Although the initial conditions remain close to the central fixed point of the α-x space, they are now chosen inside the thin stochastic layer surrounding the

primary separatrix of the β-y space. The diffusion of H_x is again caused by the small coupling to the stochastic y motion, but since thin layer trajectories are considerably less "random" than thick layer trajectories, the diffusion is significantly weaker.

An example of thin layer diffusion is shown in Fig. 16 where both the y and x motions are displayed on the same plot. The y motion is confined to its separatrix until the x motion reaches its own separatrix.

To calculate the diffusion rate, we find the energy change ΔH_x as $\phi \equiv k_y y$ swings from $\phi = -\pi$ to $\phi = +\pi$. Starting with Eq. (33) and again neglecting the first term we have

$$\frac{dH_x}{dn} = -\mu \frac{d\theta}{dn} \sin [\theta + \phi(n)] . \tag{39}$$

As before, $\theta(n)$ corresponds approximately to small librations. But instead of randomizing $\phi(n)$ with each bounce, we now assume that it evolves very much like the phase on a pendulum separatrix.

$$\theta(n) = \theta_o \sin [\omega_x (n + n_o)] \tag{40}$$

$$\phi(n) = 4 \tan^{-1} \left(e^{\omega_y n} \right) - \pi \tag{41}$$

where ω_x and ω_y are the frequencies of small oscillations about the central fixed points of the α-x and β-y spaces, respectively. Let

$$\omega_x = 2k_x \sqrt{a_x h} \quad , \quad \omega_y = 2k_y \sqrt{a_y h}$$

and defining

$$s \equiv \omega_y n \quad , \quad r \equiv \frac{\omega_x}{\omega_y} \tag{42}$$

then

$$\Delta H_x = \mu\theta_o r \int_{-\infty}^{+\infty} ds\ I(s)$$

where

$$I = \cos\ [r(s+s_o)]\ \sin\left\{\theta_o\ \sin\ [r(s+s_o) + \phi]\right\} \quad . \tag{43}$$

Using $\theta_o \ll 1$

$$I = \cos\ [r(s+s_o)]\ \sin\ \phi \ . \tag{44}$$

Only the symmetric part contributes to the integral.

$$I_{sym} = \frac{1}{2}\ \sin\ (rs_o)\ [\cos\ (\phi + rs) - \cos\ (\phi - rs)] \quad . \tag{45}$$

Thus,

$$\Delta H_x = \frac{1}{2}\ \mu\theta_o r\ \sin\ (rs_o)\ [A_2(-r) - A_2(r)] \tag{46}$$

where $A_m(\lambda)$ is the Melnikov-Arnold integral[7]

$$A_2(\pm r) = 4\pi r e^{\mp r/2}/\sinh\ (\pi r) \ . \tag{47}$$

We have finally

$$\Delta H_x = 4\pi\mu\theta_o\, r^2 \sin(rs_o) \sinh(\pi r/2)/\sinh(\pi r) \ . \qquad (48)$$

If we assume that $rs_o = \omega_x n_o$ is randomized after every half period of $\phi(n)$, then we can average ΔH_x^2 to get

$$\langle \Delta H_x^2 \rangle_{s_o} = 8\pi^2\mu^2\theta_o^2\, F(r) \qquad (49)$$

where

$$F(r) = r^4 \sinh^2(\pi r/2)/\sinh^2(\pi r) \ . \qquad (50)$$

A plot of $F(r)$ is shown in Fig. 17. It is sharply peaked close to $r = 1$, suggesting that if the characteristic frequencies of the separatrix and libration motion differ by as much as a factor of four, the diffusion will be reduced by two orders of magnitude.

To obtain the diffusion coefficient, we need to know the mean half period of the motion in the thin stochastic layer $\bar{T}_\beta$. The half period of a true pendulum that follows a trajectory very close to the separatrix is approximately

$$T_\beta = \frac{1}{\omega_y} \ell n \frac{32}{|W|} \qquad (51)$$

where

$$W \equiv \frac{H_y - H_s}{H_s} \ll 1 \ ,$$

and

$$H_s = \frac{\omega_y^2}{h}$$

is the separatrix energy. Chirikov[8] has shown that the average half period inside the stochastic layer may be computed by simply integrating the half period over the energy interval of the layer. The result is

$$\bar{T}_\beta = \frac{1}{\omega_y} \ell n \frac{32e}{|W_o|} \tag{52}$$

where W_o is the relative energy at the edge of the layer (it has approximately the same magnitude on both sides of the separatrix) and e is the natural base. Chirikov has also calculated the layer width W_o using the so-called "whisker mapping". In our calculations, we have used actual measurements of W_o taken from computer generated plots of the uncoupled motion. The separatrix width is not appreciably affected by small couplings $\varepsilon \ll a_y$.

Combining Eqs. (49) and (52) we get the thin layer diffusion coefficient

$$D_2 = \frac{\langle \Delta H_x^2 \rangle_{s_o}}{2\bar{T}_\beta} \tag{53}$$

or

$$D_2 = 4\pi^2 \mu^2 \theta_o^2 \omega_y \, F(r)/\ell n \, (32e/|W_o|) \, . \tag{54}$$

In Fig. 18, the theoretical thin layer diffusion is compared with experimental measurements. Each triangle represents the final spread of 100 particles that have been started with identical initial conditions in the α-x space and slightly different initial conditions in the thin stochastic layer of the β-y space. The motion was followed for 2000 iterations and the RMS spread was computed using

$$\alpha^2_{RMS} = \left(\frac{1}{100}\sum_{i=1}^{100}\left(\overline{\alpha^2} - \alpha_i^2\right)\right)^{\frac{1}{2}} \tag{55}$$

The theoretical curves were calculated from Eq. (54) with $W_o = .191$. The variation of $\left(\alpha^2\right)_{RMS}$ with coupling strength is shown in Fig. 18a. Variations with ω_x and n are shown in Figs. 18b and 18c, respectively. Again, the theoretical values fall slightly above the experimental, probably due to the fact that the y motion phase $\phi(n)$ is not completely randomized with each successive half period of the separatrix motion. Phase correlations have been observed[10] in a similar mapping for the Fermi problem. Nevertheless, theory and experiment agree surprisingly well, lending considerable support to the validity of the "stochastic pump" model of the Arnold diffusion.

V. CONCLUSION

Any near-integrable system with N degrees of freedom and $M < N - 1$ global invariants of the motion will exhibit Arnold diffusion. Diffusion occurs on the stochastic layers that form around the separatrices of resonant trajectories. The resonant action associated with a particular layer is approximately conserved by diffusion along that layer (and may be mistaken for an additional true invariant).

We have calculated diffusion rates for two types of diffusion using the simple model of a particle bouncing between a flat and a periodically rippled wall. Both processes are strongly dependent upon the ratio of the characteristic frequencies of the stochastic layer and the diffusing oscillations. Thick layer diffusion tends to be much faster than thin layer diffusion due to the more frequent phase randomizations in the former. The excellent agreement between theory and computer simulation supports the "stochastic pump" model of the Arnold diffusion.

ACKNOWLEDGMENTS

We are especially in debt to B. V. Chirikov for providing us with many of the concepts and techniques used in this paper. This work was supported under National Science Foundation Grant ENG78-09424 and Department of Energy Contract EY-76-S-03-0034-PA215.

REFERENCES

1. A. M. Vinogradov and B. A. Kupershmidt, Russ. Math. Surveys 32, 177 (1977).
2. M. Toda, "Studies of a Nonlinear Lattice," Phys. Reports 18c, 3 (1975). See also, M. V. Berry, "Regular and Irregular Motion" in Nonlinear Dynamics, Am. Inst. Phys. Conf. Proc. Series Vol. 46, A.I.P. New York (1978).
3. E. T. Whittaker, A Treatise on the Analytical Dynamics of Particles and Rigid Bodies, (Cambridge University Press, fourth edition, London 1937), p 313-314.
4. C. L. Siegal, Ann. Math. 42, 806 (1941) Math. Anal. 128, 144 (1954).
5. A. N. Kolmogorov, Dokl. Akad. Nauk SSSR 98 (1965) 527.
6. V. I. Arnold, A. Avez, Ergotic Problems of Classical Mechanics (Benjamin, Inc., New York, 1968).
7. V. I. Arnold, Dokl. Akad. Nauk SSSR 156, 9 (1964).
8. B. V. Chirikov, "A Universal Instability of Many Dimensional Oscillator Systems", Institute of Nuclear Physics, 630090 Novosibirsk, USSR.
9. G. Contopoulos, L. Galgani and A. Giorgilli, "On the Number of Isolating Integrals in Hamiltonian Systems" ESO Preprint n. 26, submitted to Phys. Rev. A (1978).
10. C. Froeschlé, Astrophs. Space Sci. 14, 110 (1971); C. Froeschlé and J. P. Scheidecker, Astrophys. Space Sci. 25, 373 (1973).
11. V. K. Melnikov, Dokl. Akad. Nauk SSSR 144, 747 (1962); 148, 1257 (1963); Trudy Moskovskova Mat. Obschestra 12, 3 (1963). See also Ref. 7 and Ref. 8 (Appendix).

12. See Ref. 8, Sections 4.4 and 6.1.

13. M. A. Lieberman and A. J. Lichtenberg, Phys. Rev. 45, 1852 (1972).

FIGURE CAPTIONS

Fig. 1 The free particle is perturbed by a periodic perturbation in three dimensions.

Fig. 2 Resonance vectors $\underline{m}$ in action space (also frequency and velocity space). The vectors are normalized to unity and projected at an oblique angle. All vectors with $|m_i| \leq 2$ are shown.

Fig. 3 The Arnold web. The intersection of resonance planes with the energy surface in action space. The lines shown correspond to $|m_i| \leq 2$.

Fig. 4 The energy surface, resonance vector, resonance line, frequency vector and change in action for a free particle perturbed by a single wave.

Fig. 5 Thickening of the action surface, libration, separatrix, and rotation motion for a single wave perturbation.

Fig. 6 Action (frequency, velocity) space for the two wave system showing the primary resonances and the network of secondary resonances.

Fig. 7 Confinement of stochastic trajectories for the two wave system. Motion is confined to the intersection of the $\underline{n}$-$\underline{\ell}$ plane with the energy surface.

Fig. 8 Action space for the three wave system, showing the three primary resonances and the network of secondary resonances — the Arnold web.

Fig. 9 The three dimensional billiards problem. A point particle bounces back and forth between a smooth and a periodically rippled wall.

Fig. 10 Motion in two degrees of freedom, illustrating the definition of the trajectory angle α_n , and the bounce position x_n just before

the $n^{\underline{th}}$ collision with the wall. $\alpha = \arctan(v_x/v_z)$, $\beta = \arctan(v_y/v_z)$.

Fig. 11 Motion in the α-x surface of section for the uncoupled billiards problem described by the simplified Eqs. (18)-(24). The parameters are $\varepsilon = 0$; λ_x:h:a_x as 100:10:2 ; $\lambda_x = 2\pi/k_x$. 15 particles are started at $x = 0$ and allowed to run for 1000 iterations each.

Fig. 12 Exact motion for the uncoupled billliards problem. Same parameters as Fig. 11.

Fig. 13 Integrable motion in the coupled billiards problem. Motion is projected onto the α-x surface of section. The projection onto the β-y surface is qualitatively the same. Parameters are $\varepsilon/h = .004$; λ_x:h:a_x and λ_y:h:a_y as 100:10:2 .

Fig. 14 Thick layer diffusion for the coupled billiards problem. Initial conditions are close to the central "fixed point" in the α-x space and within the thick stochastic layer (near $|\beta| = \pi/2$) of the β-y space. Parameters are the same as Fig. 13.

Fig. 15 Thick layer diffusion. Comparison of the theoretical diffusion, Eq. (38) with the results of simulation experiments. In a), the dispersion is plotted vs the coupling amplitude, ε . In b), dispersion vs the libration period, T_a . In c), dispersion vs the number of iterations, n . Parameters (except for those varied) are $\varepsilon/h = .0001$; $n = 500$; λ_x:h:a_x as 10:10:1 ; λ_y:h:a_y as 100:10:1.7 . Each triangle gives the spread of 100 particles.

Fig. 16 Thin layer diffusion. Initial conditions are close to the central fixed point in the α-x space and within the separatrix stochastic layer in the β-y space. Parameters are the same as Fig. 13.

Fig. 17 Plot of the function

$$F(r) = \frac{r^4 \sinh^2\left(\frac{\pi r}{2}\right)}{\sinh^2 \pi r}$$

for the dependence of thin layer diffusion on $r = \omega_x/\omega_y$.

Fig. 18 Thin layer diffusion. Comparison of the theoretical diffusion, Eq. (54) with the results of simulation experiments. The three graphs are the same relations as those shown in Fig. 15. Parameters (except for those varied) are $\varepsilon/h = .0001$; $n = 2000$; $\lambda_x : h : a_x$ as 100:10:1 ; $\lambda_y : h : a_y$ as 100:10:1.8 . Each triangle gives the spread of 100 particles.

FIGURE 1.
A periodic lattice
in 3 dimensions

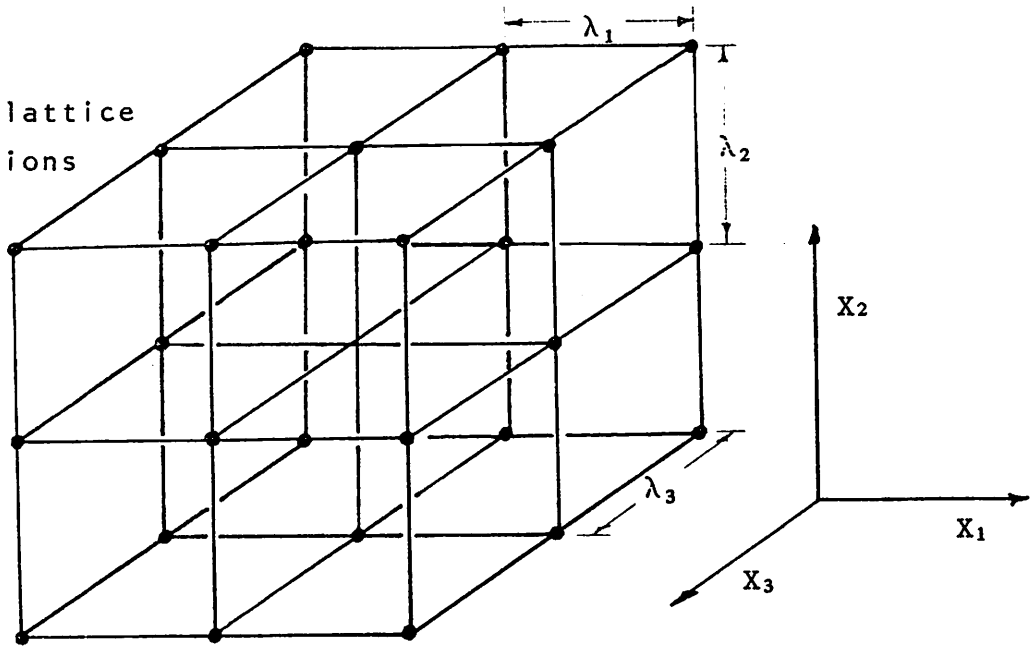

FIGURE 2.
Resonance
vectors

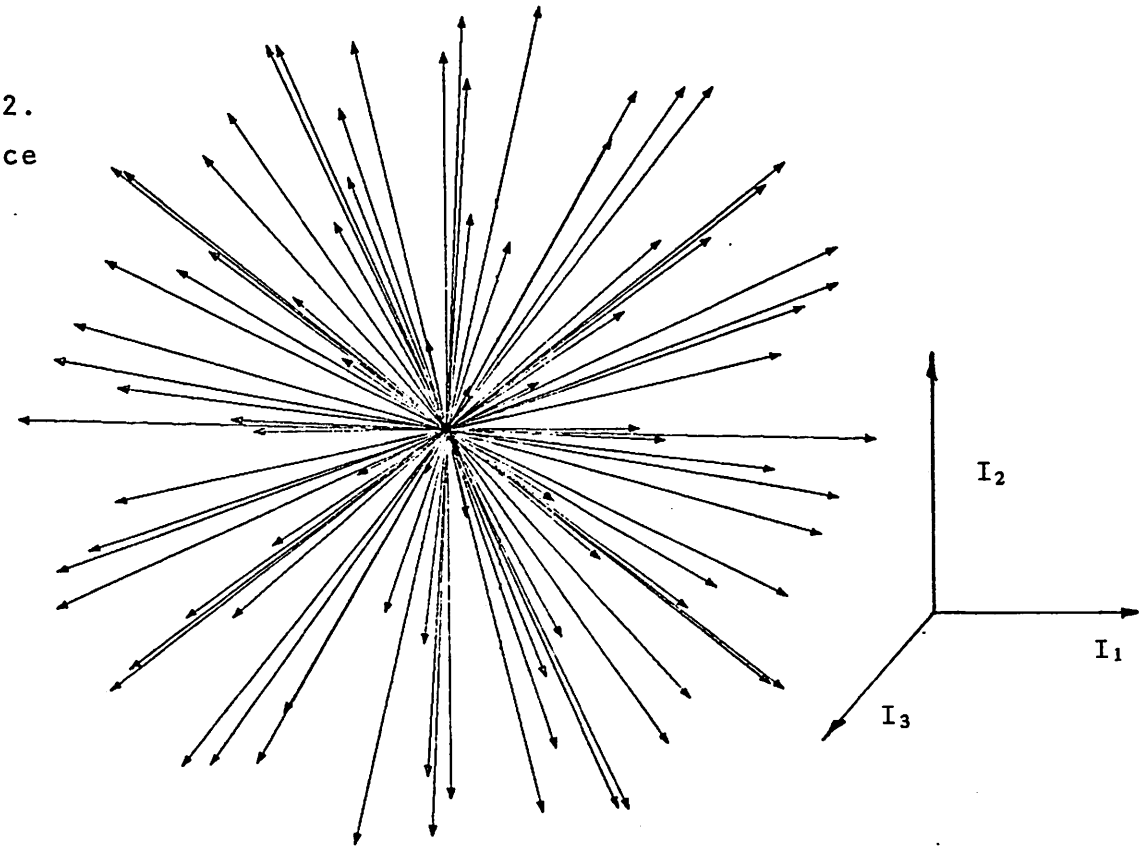

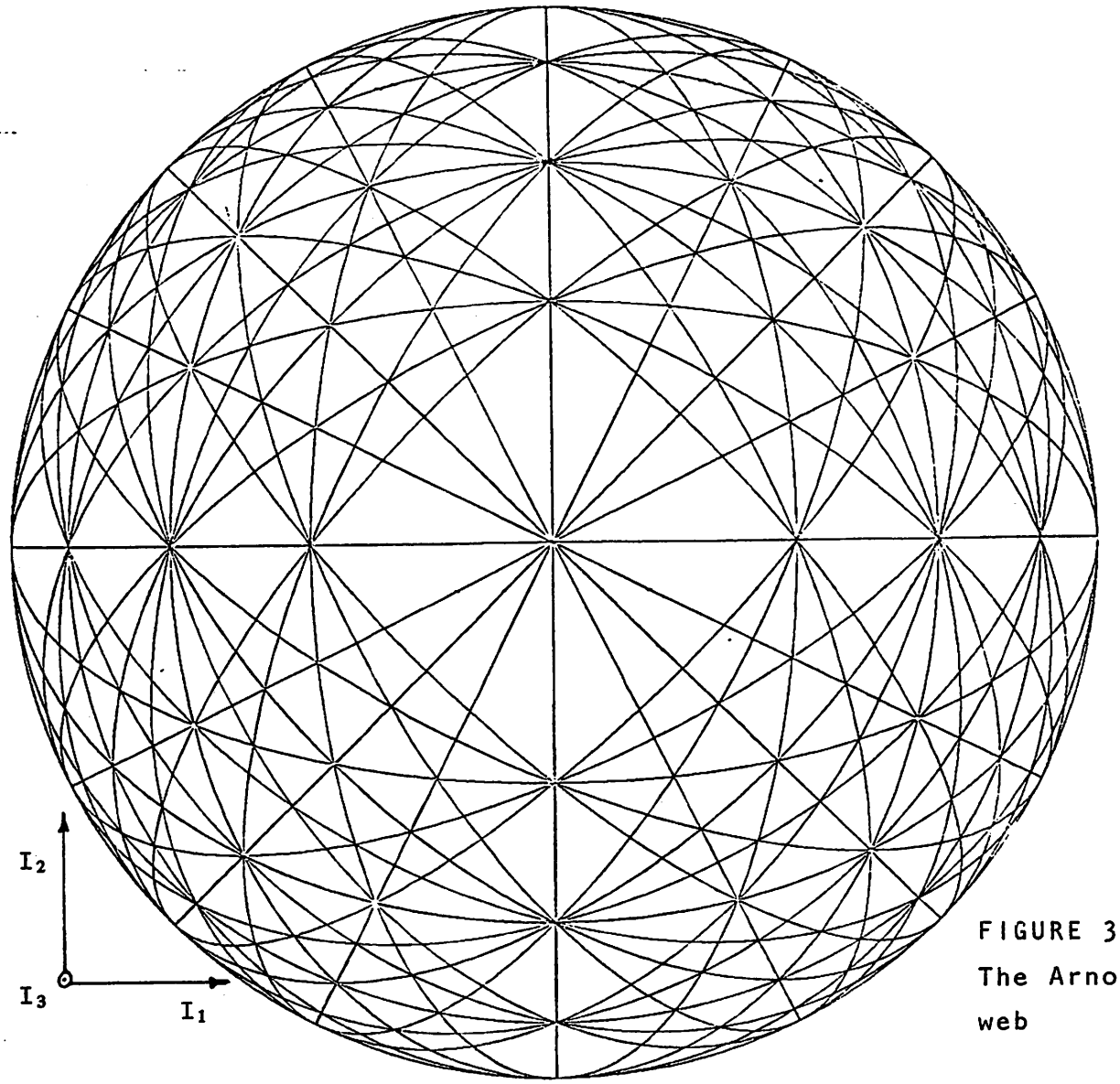

FIGURE 3.
The Arnold web

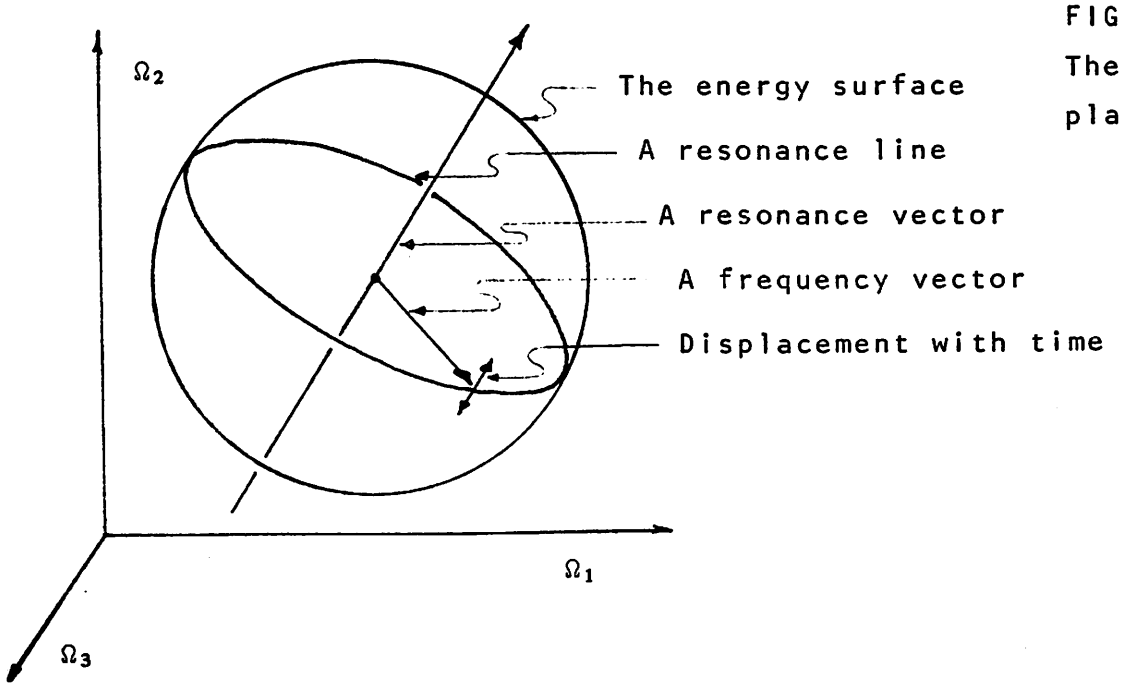

FIGURE 4.
The resonance plane

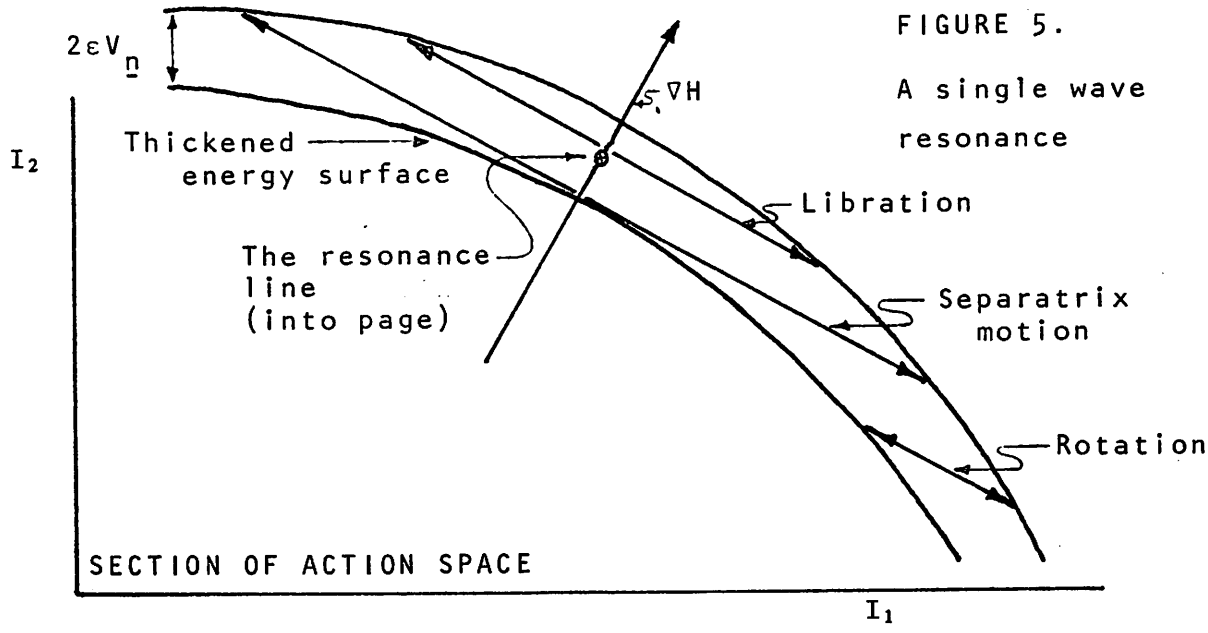

FIGURE 5.

A single wave resonance

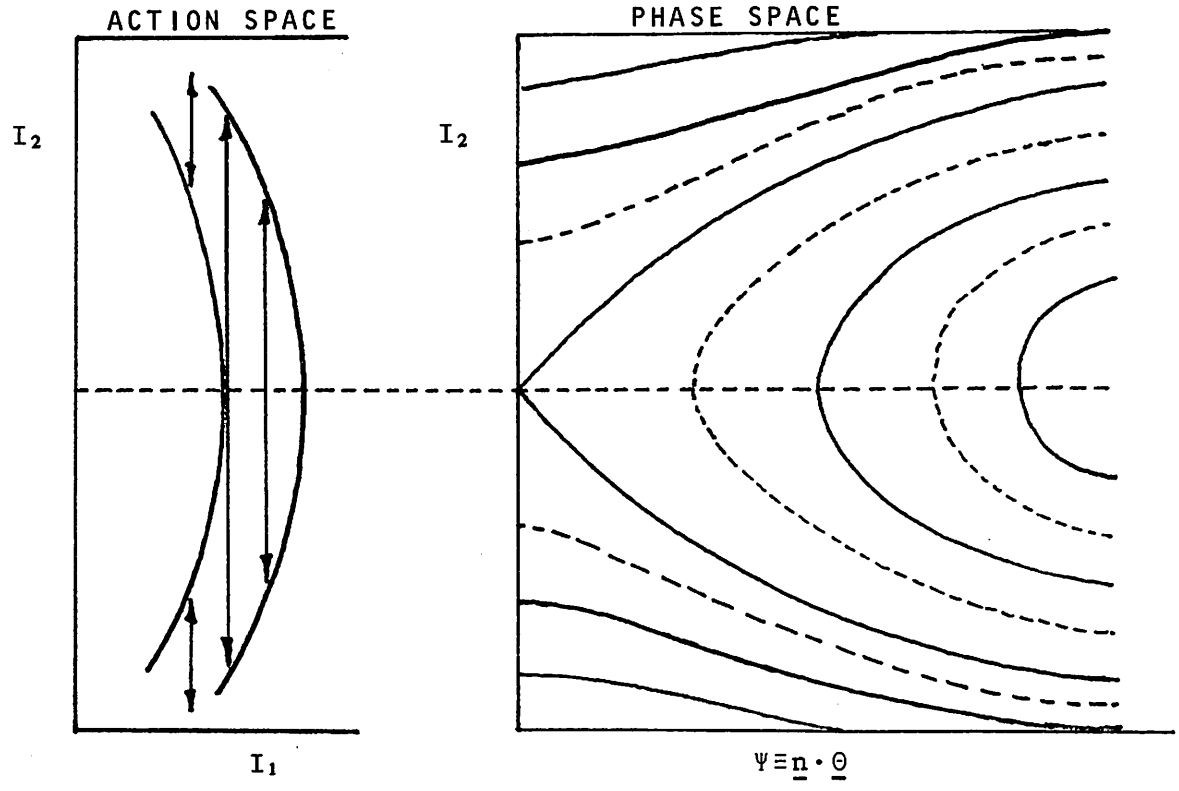

FIGURE 6.
Resonance lines
for two waves

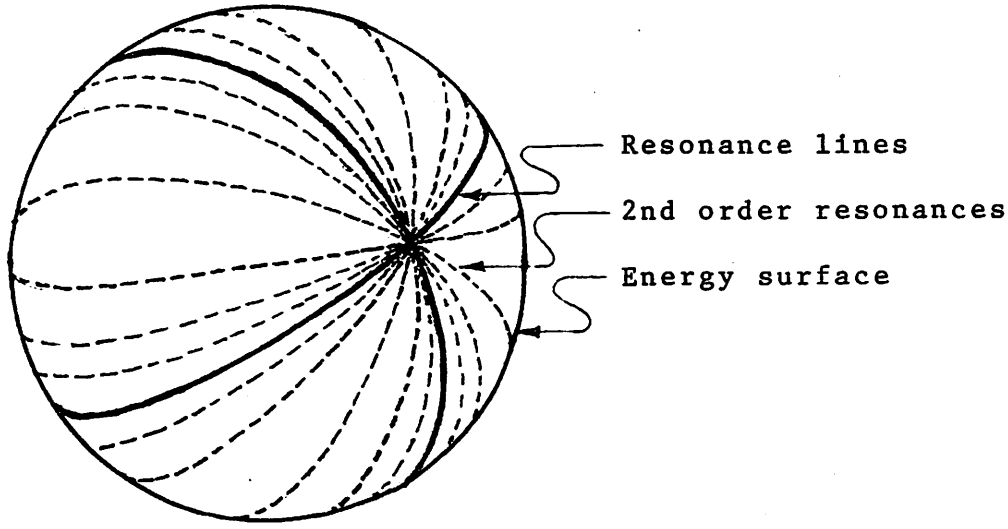

FIGURE 7.
Confinement of stochastic
trajectories for two
waves

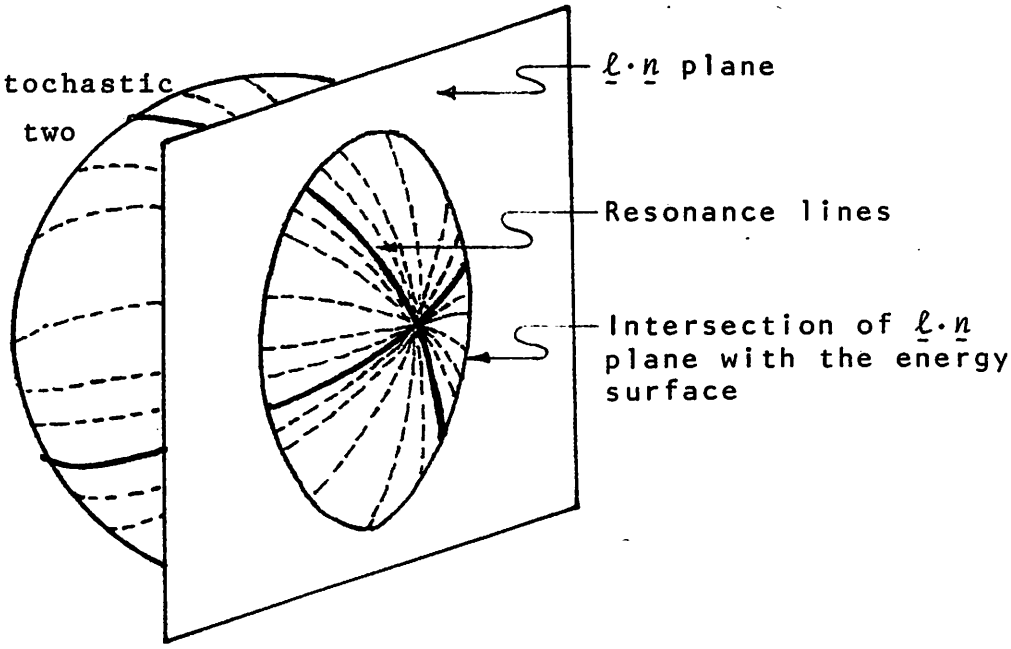

FIGURE 8.
Resonance lines
for three waves

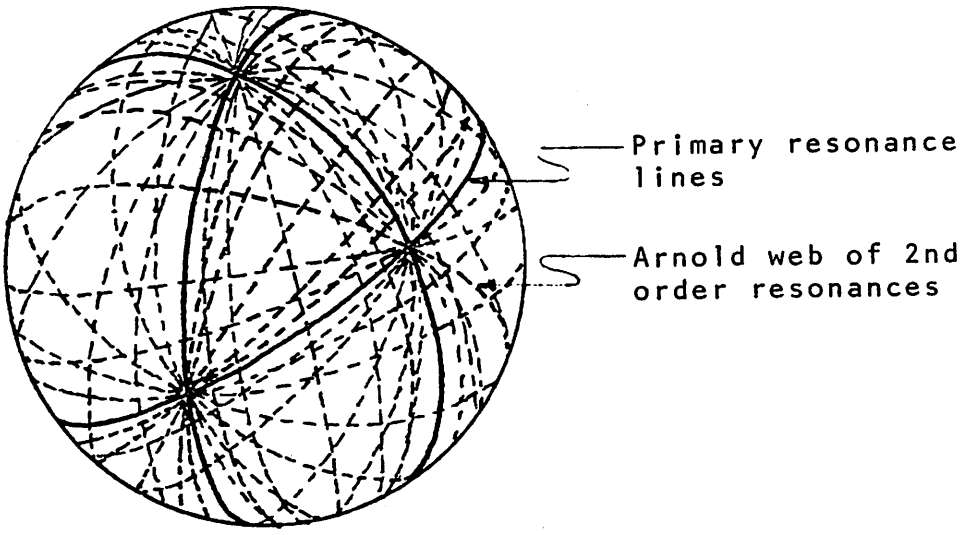

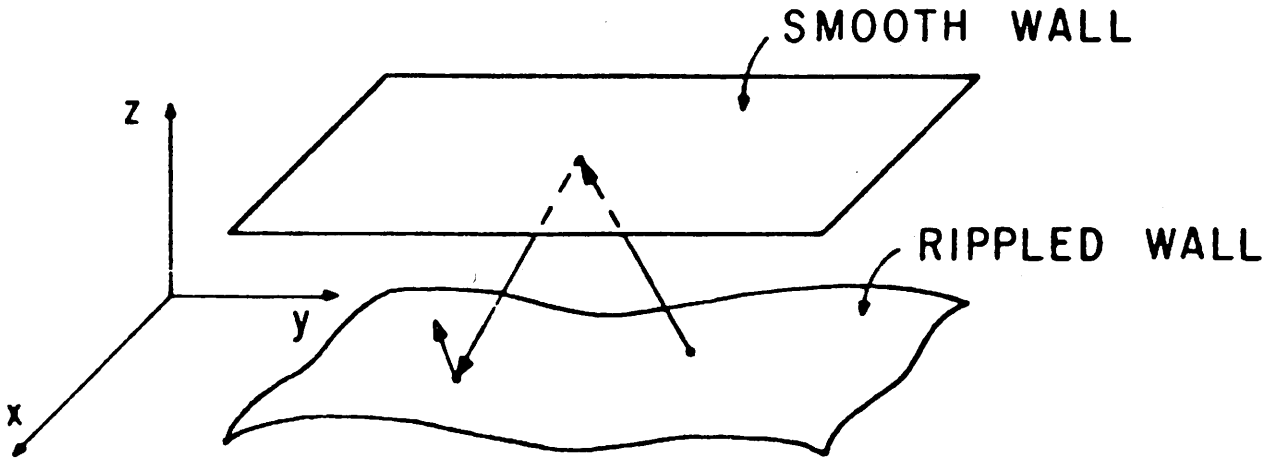

FIGURE 9.
The three dimensional
billiards problem

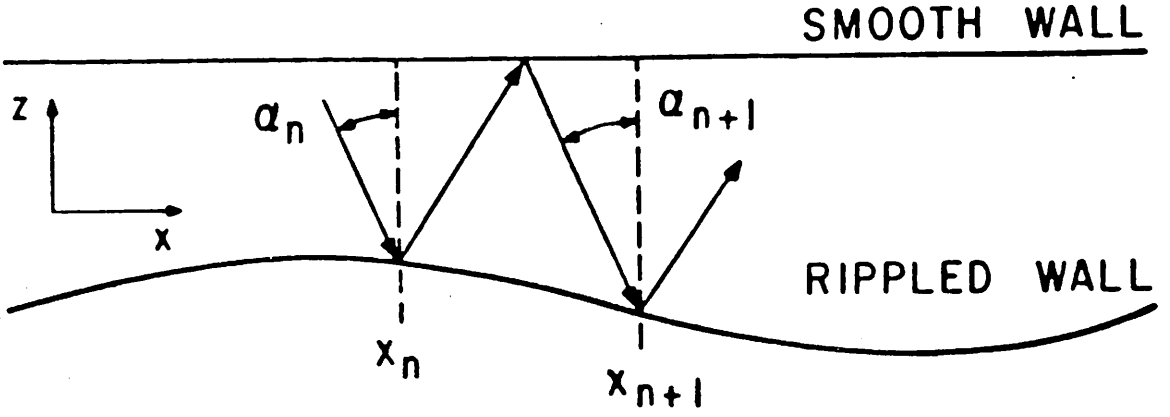

FIGURE 10.
The definitions of α_n and x_n

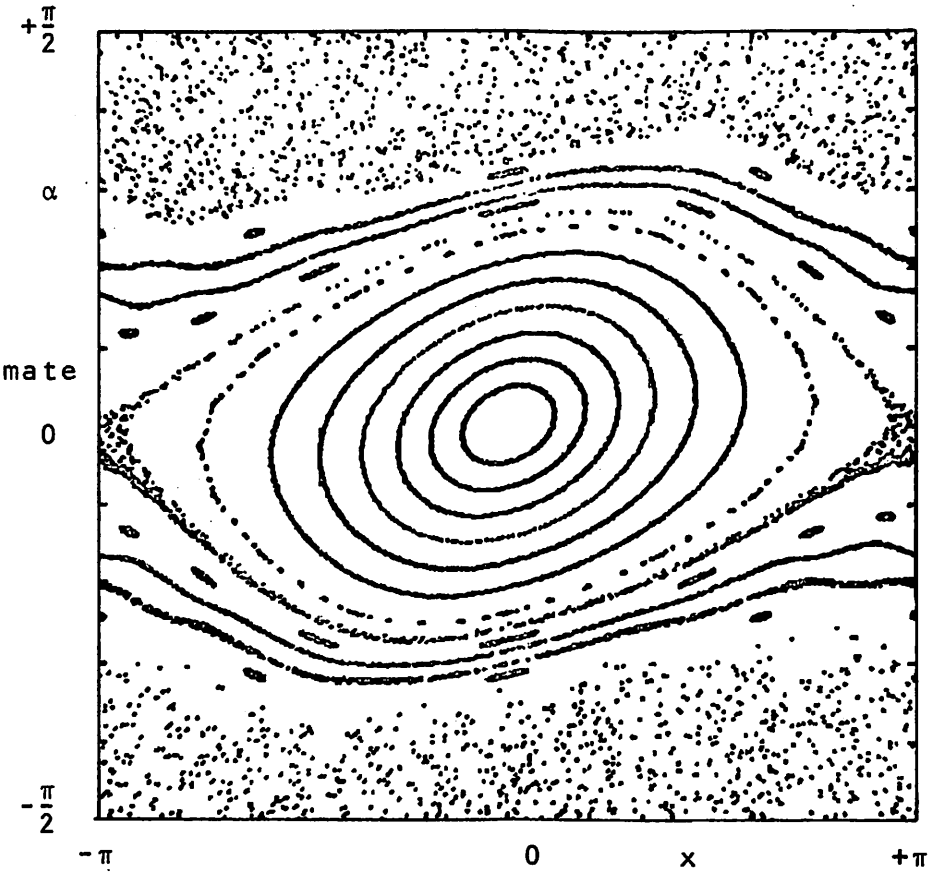

FIGURE 11.
The approximate difference equations

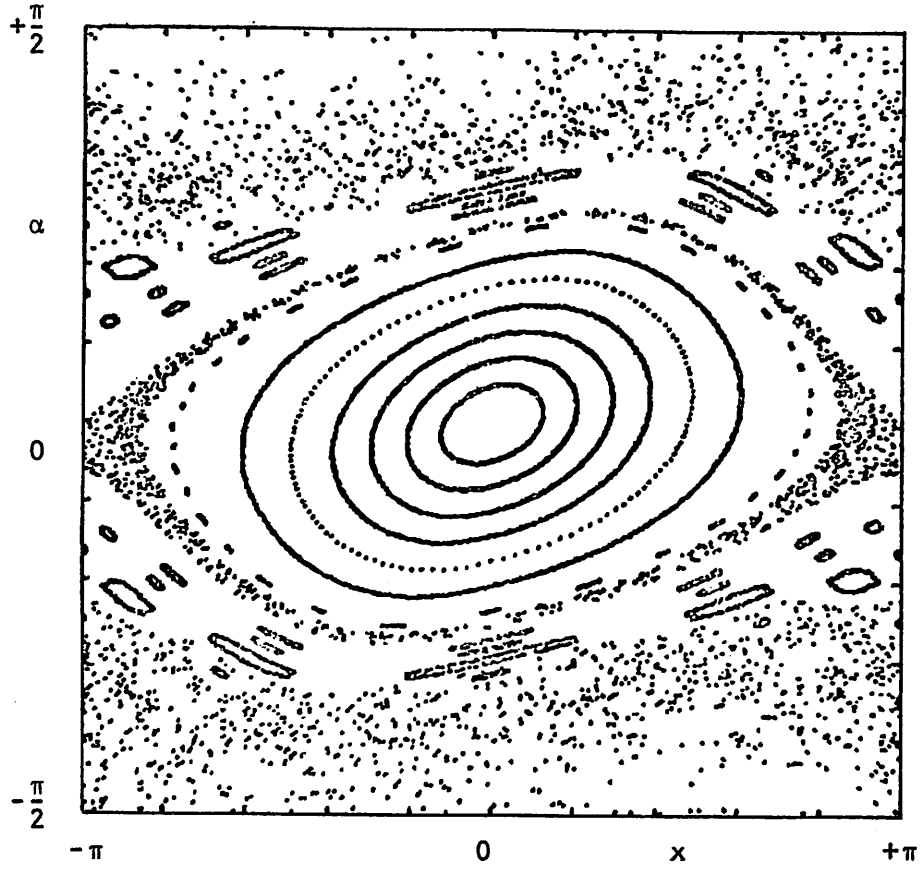

FIGURE 12.
The exact problem

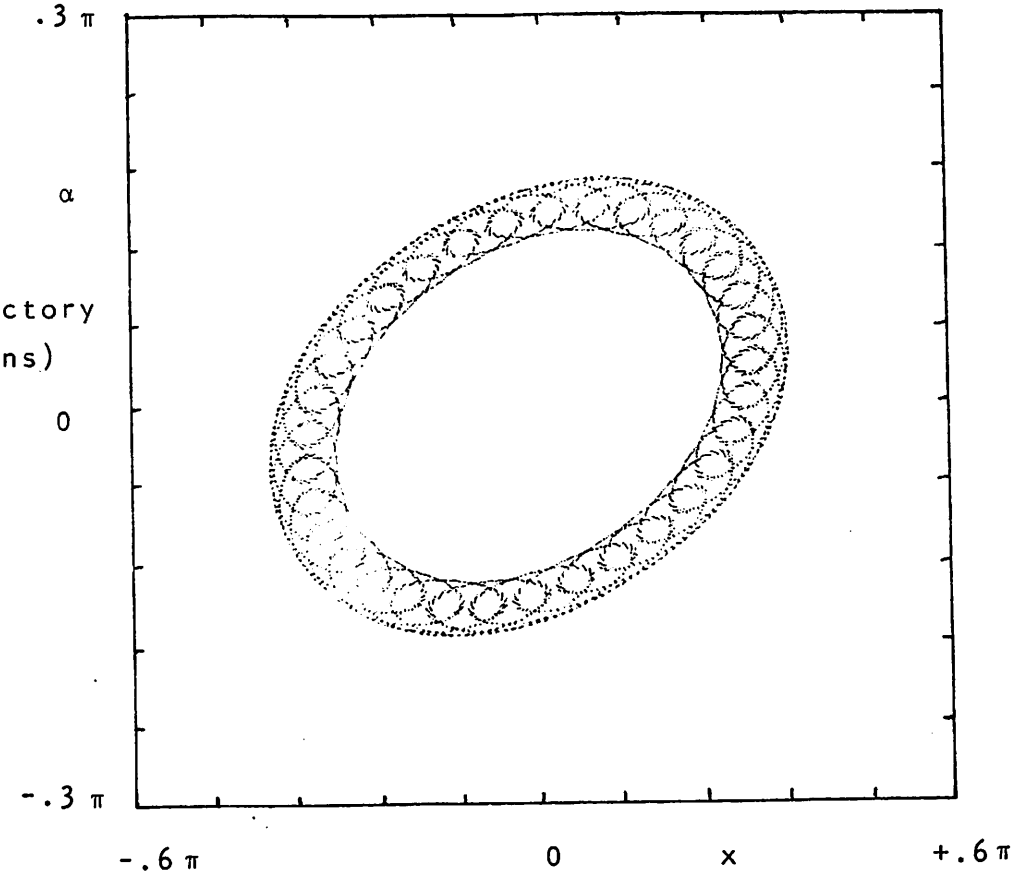

FIGURE 13a.
A stable trajectory
(5000 iterations)

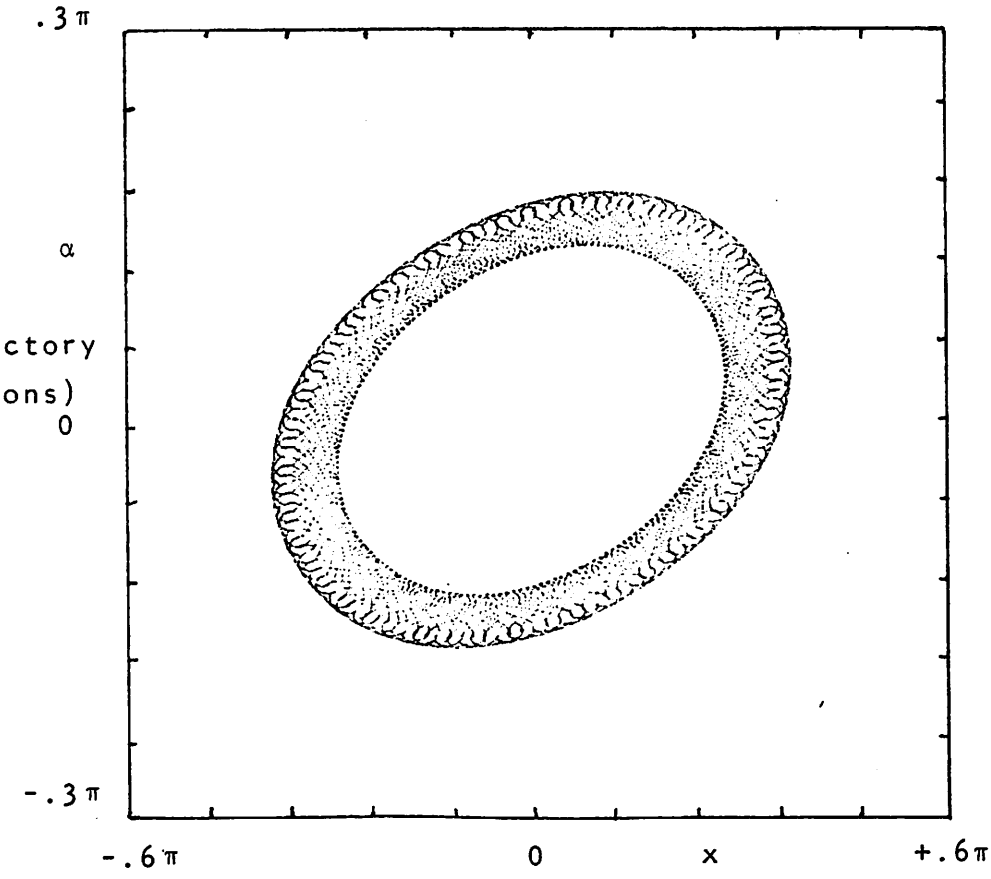

FIGURE 13b.
A stable trajectory
(50000 iterations)

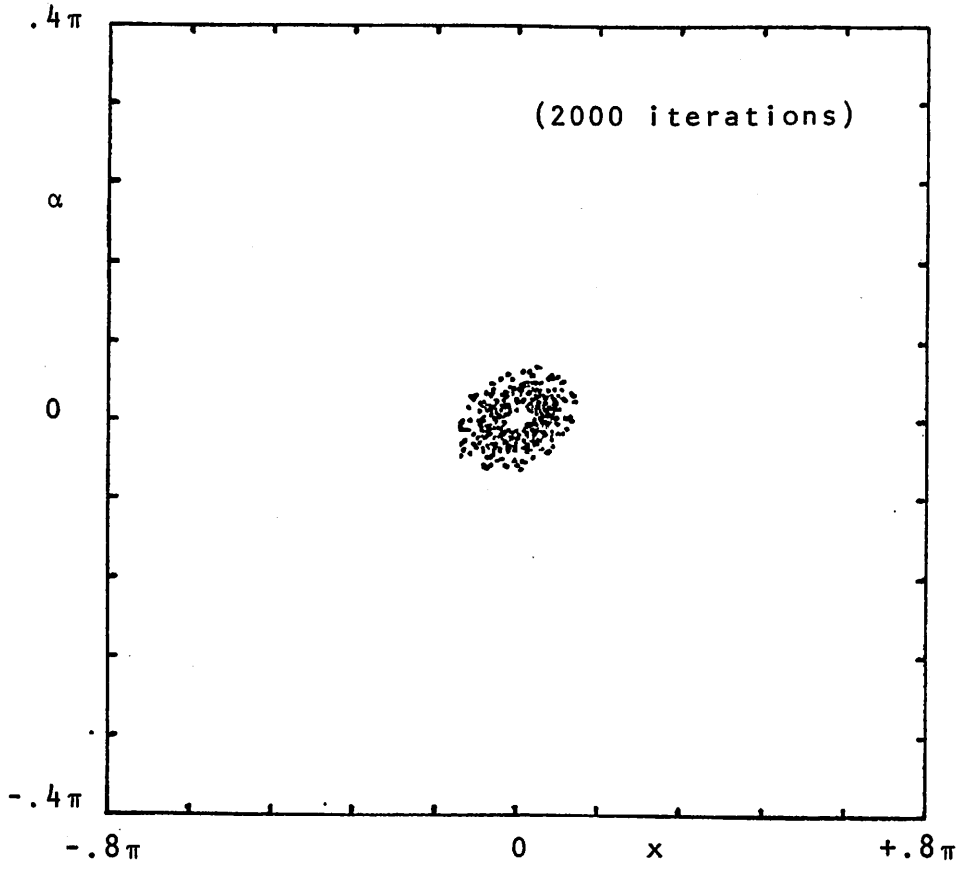

FIGURE 14.

Thick layer diffusion

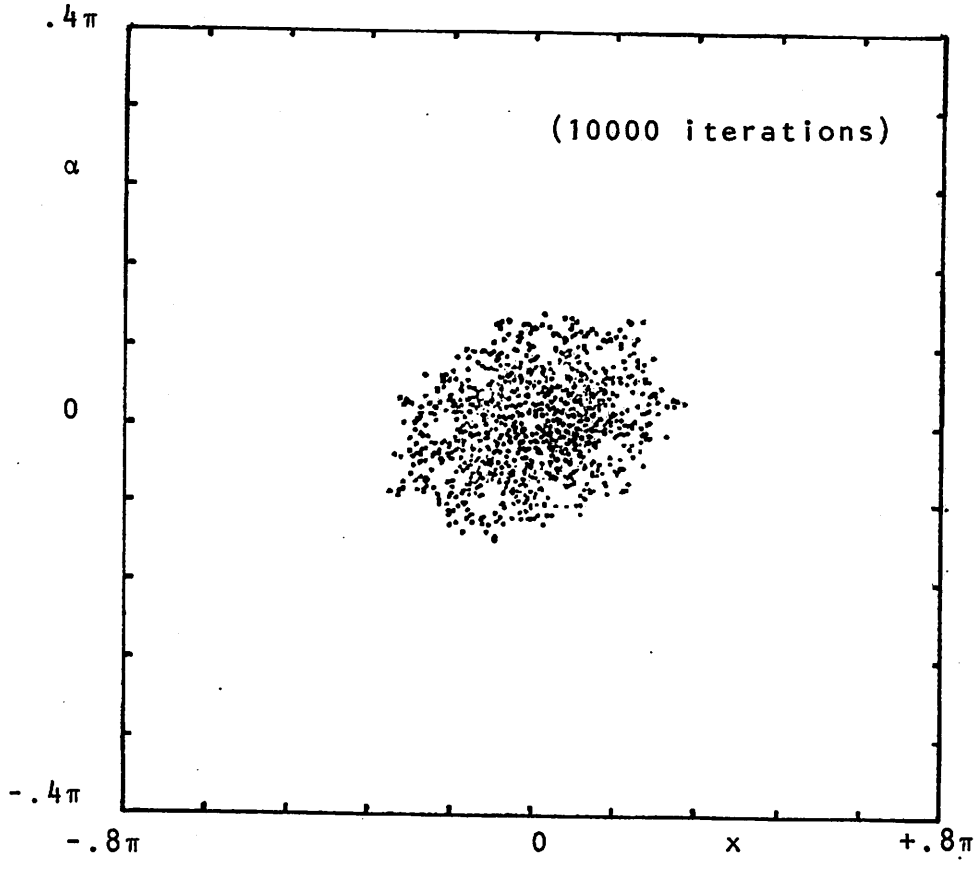

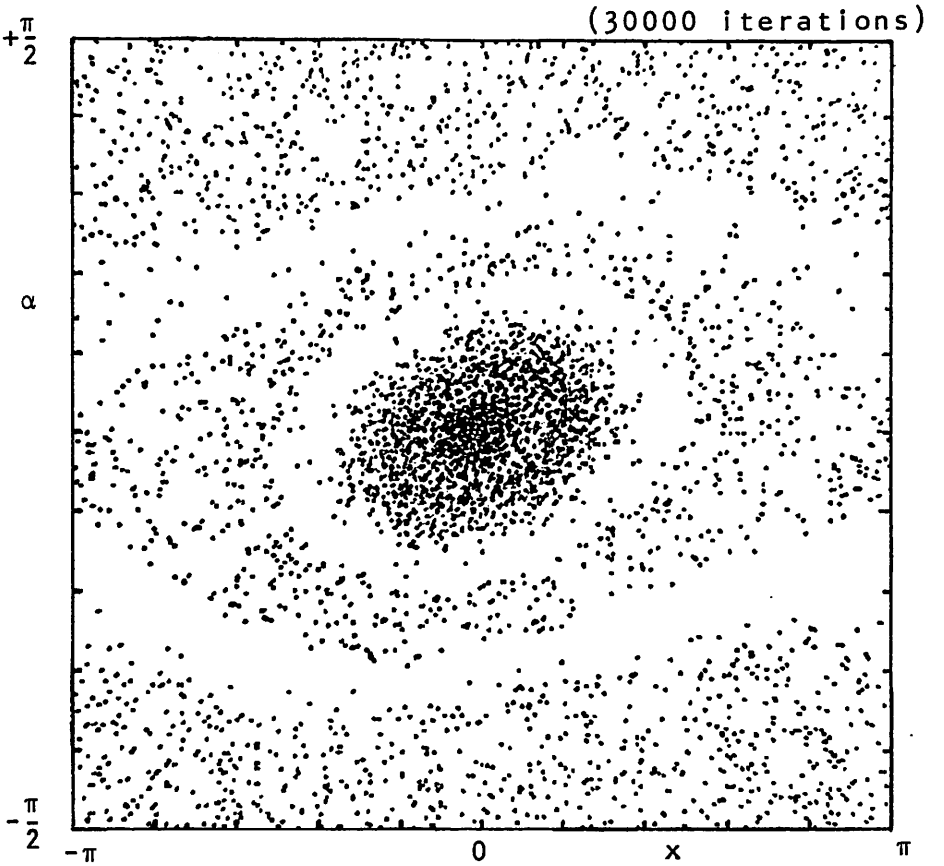

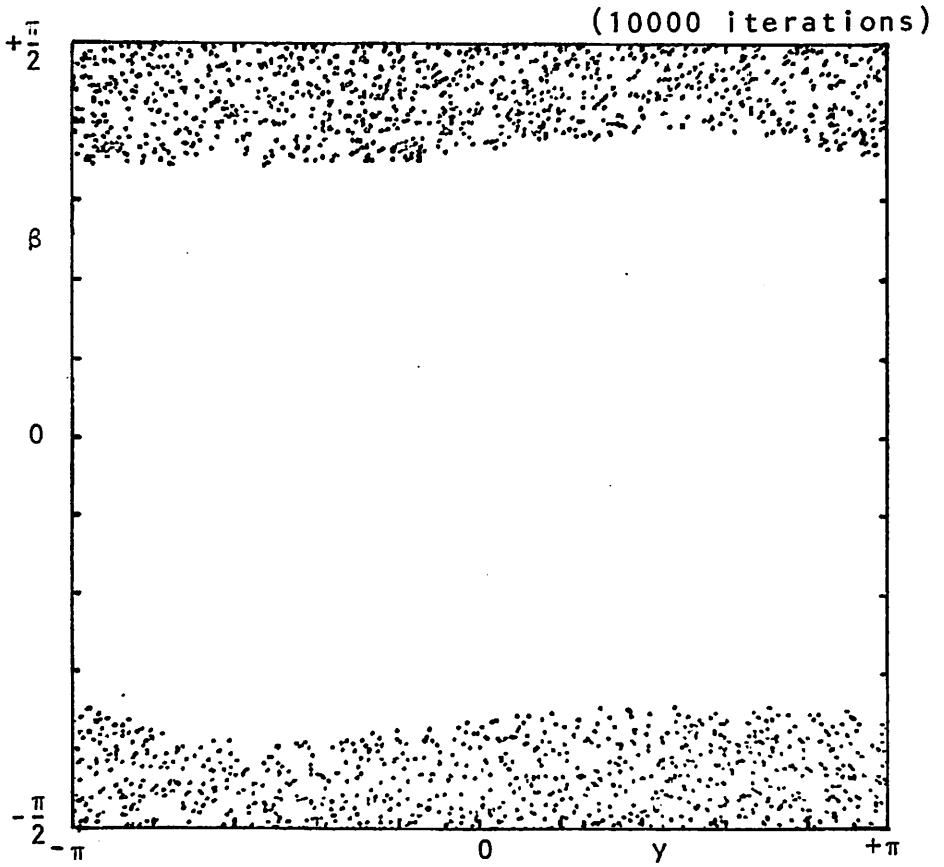

FIGURE 14. cont.
Thick layer
diffusion

FIGURE 15.

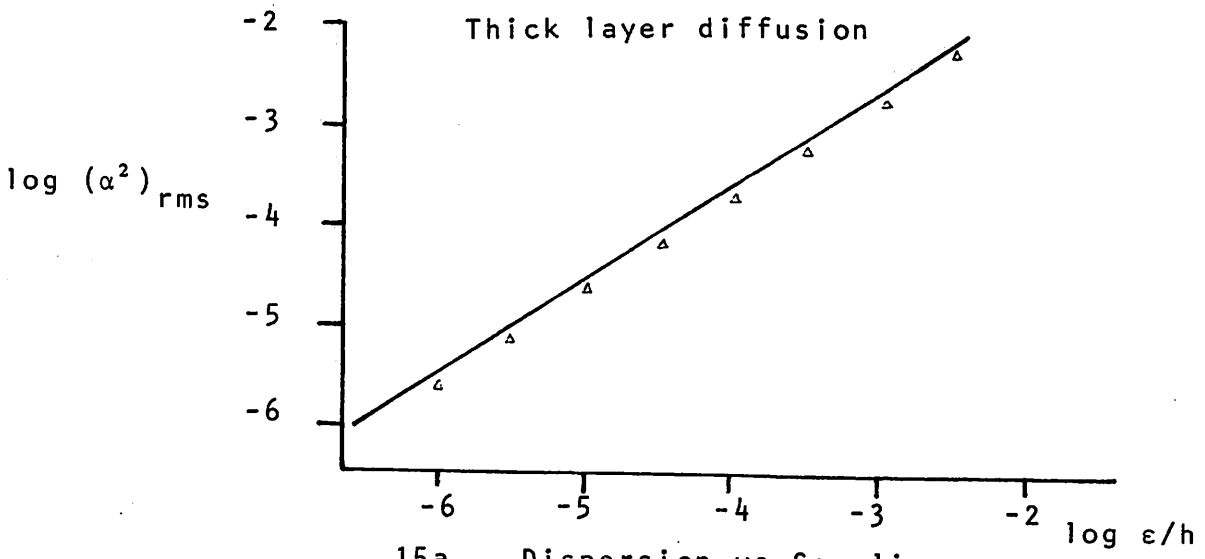

15a. Dispersion vs Coupling

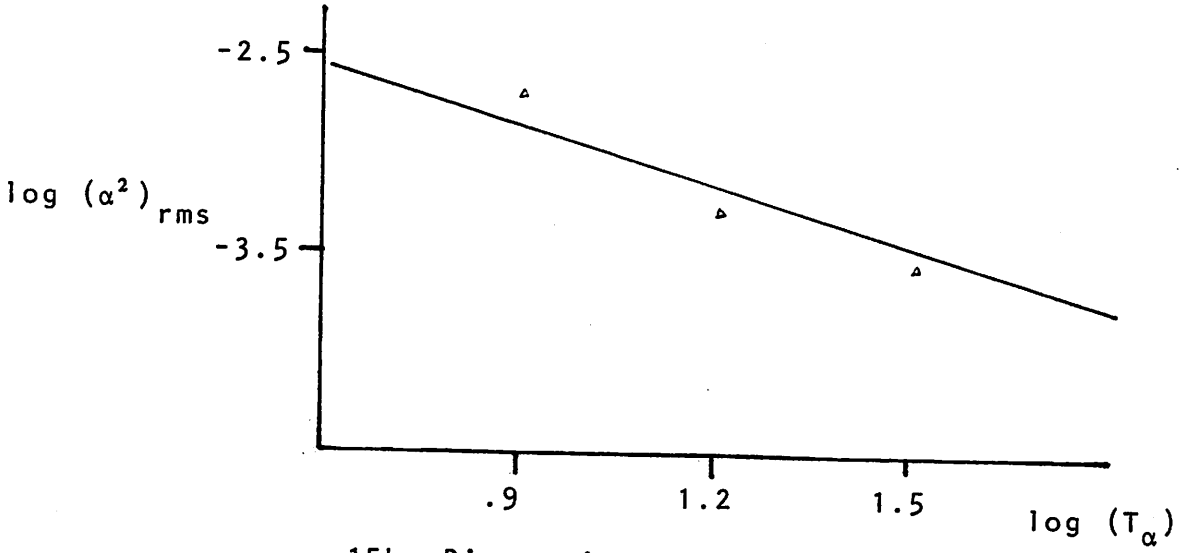

15b. Dispersion vs Libration Period

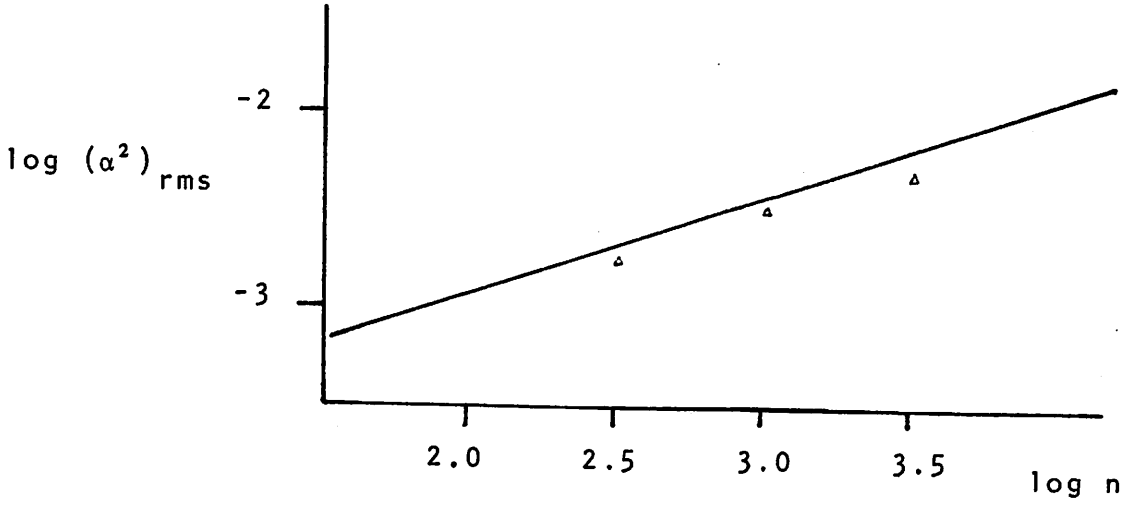

15c. Dispersion vs Iteration Number

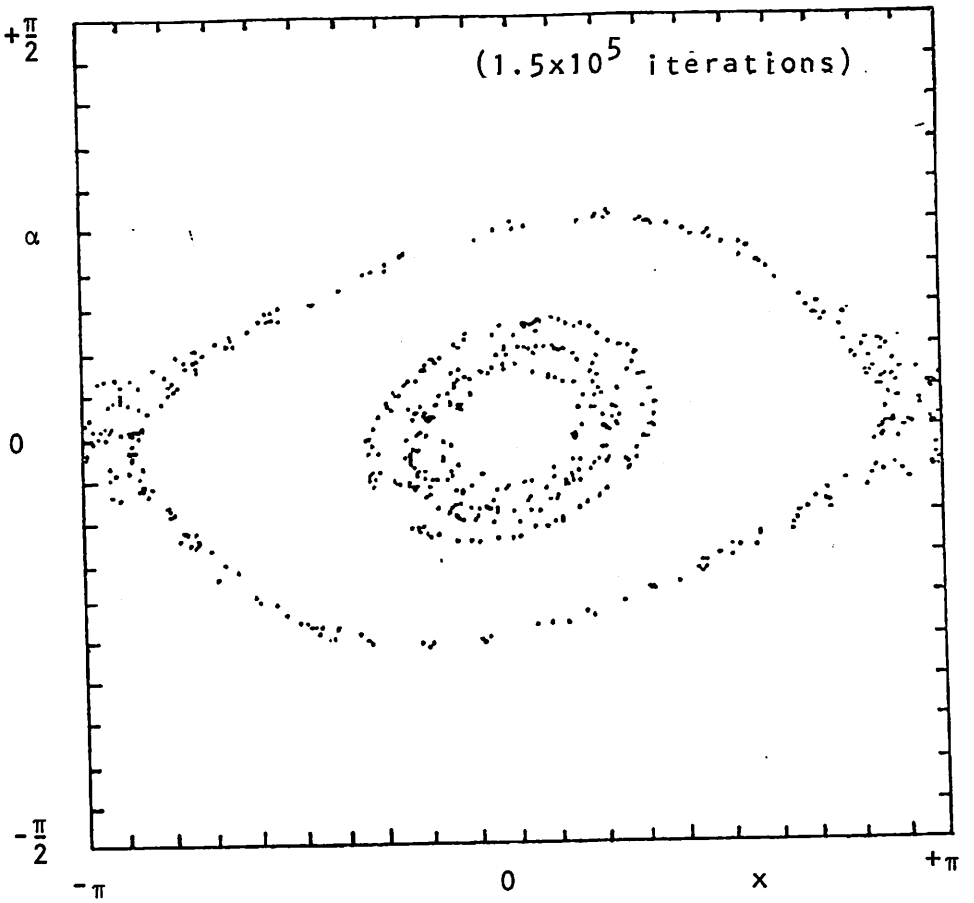

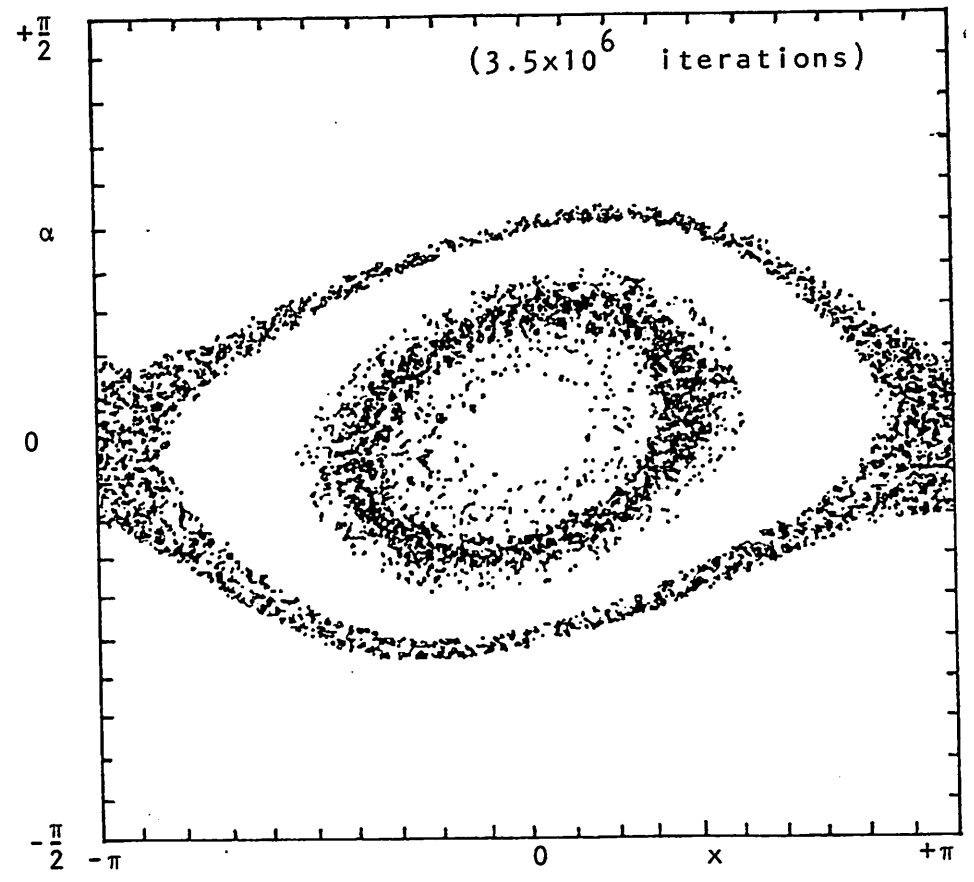

FIGURE 16. Thin layer diffusion

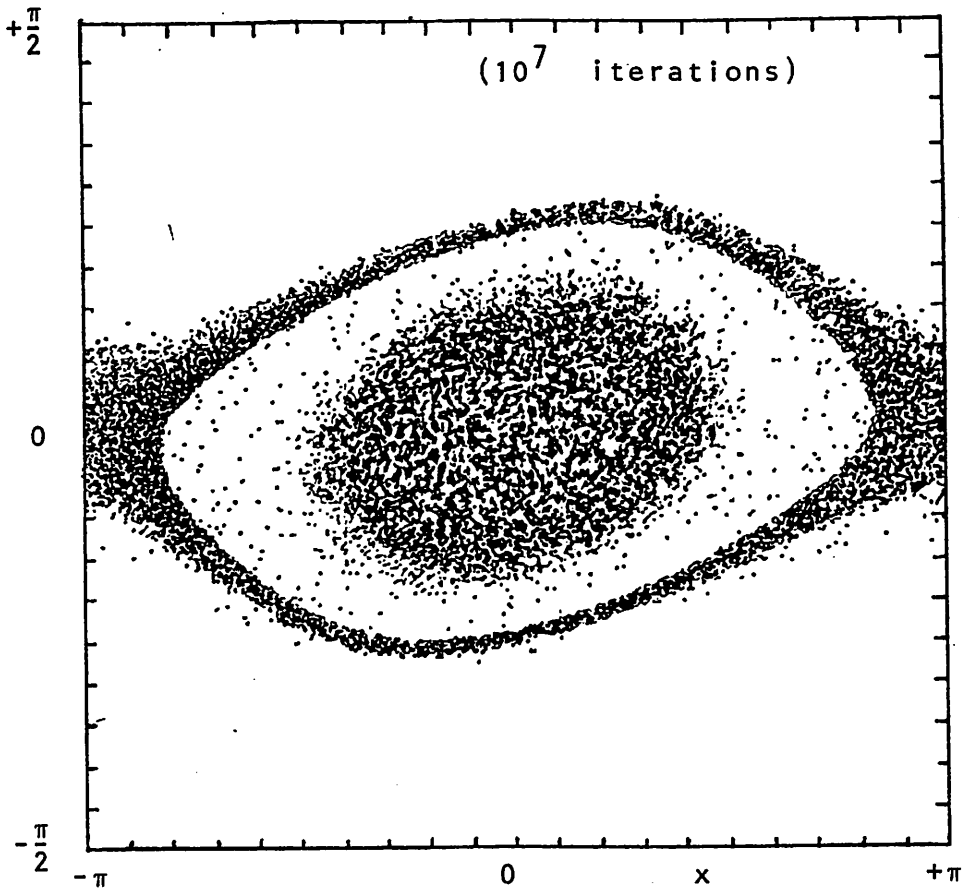

FIGURE 16. cont.
Thin layer diffusion

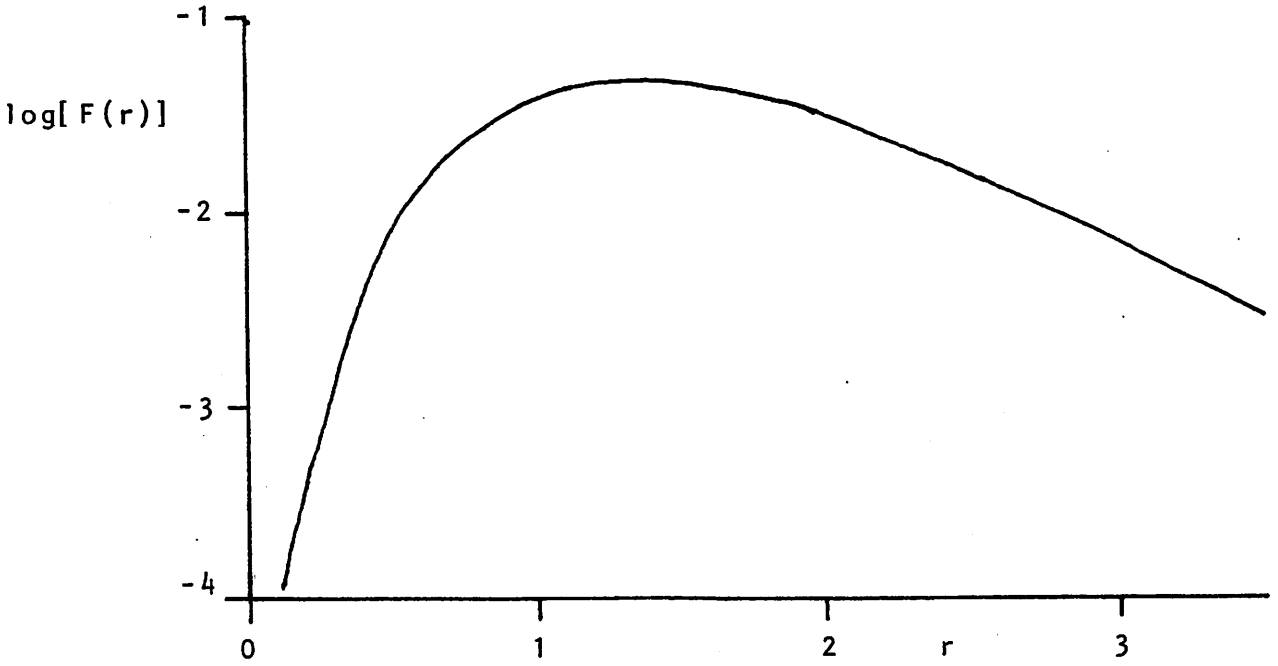

FIGURE 17.
Plot of F(r)

FIGURE 18.

Thin layer diffusion

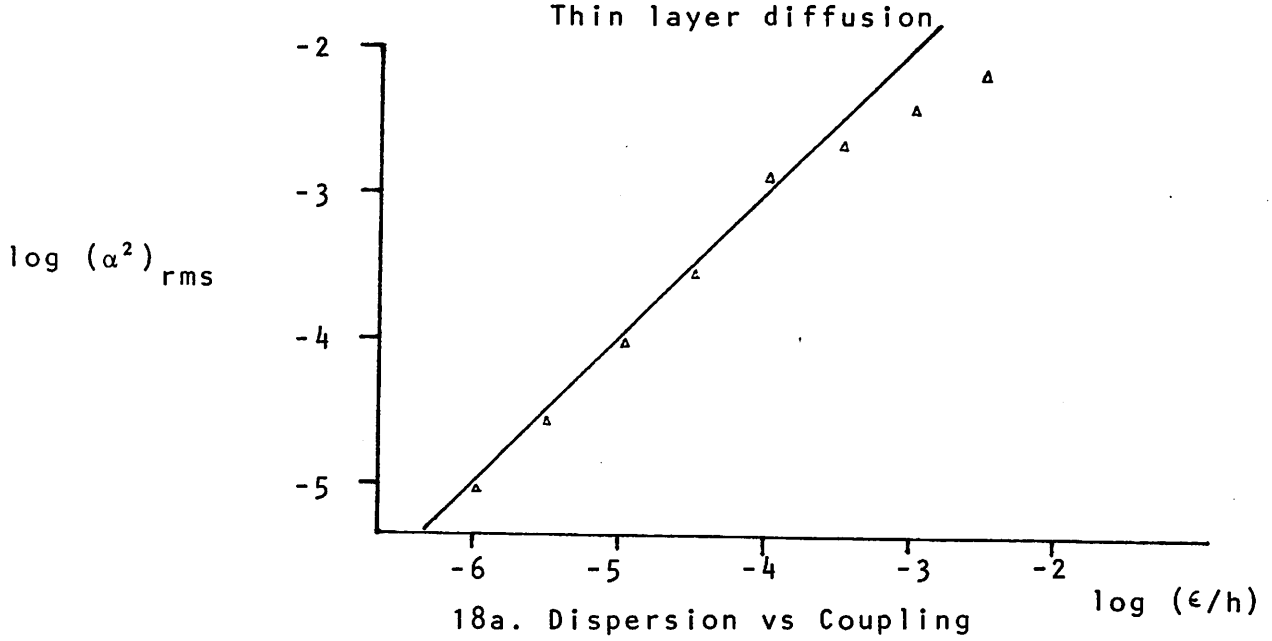

18a. Dispersion vs Coupling

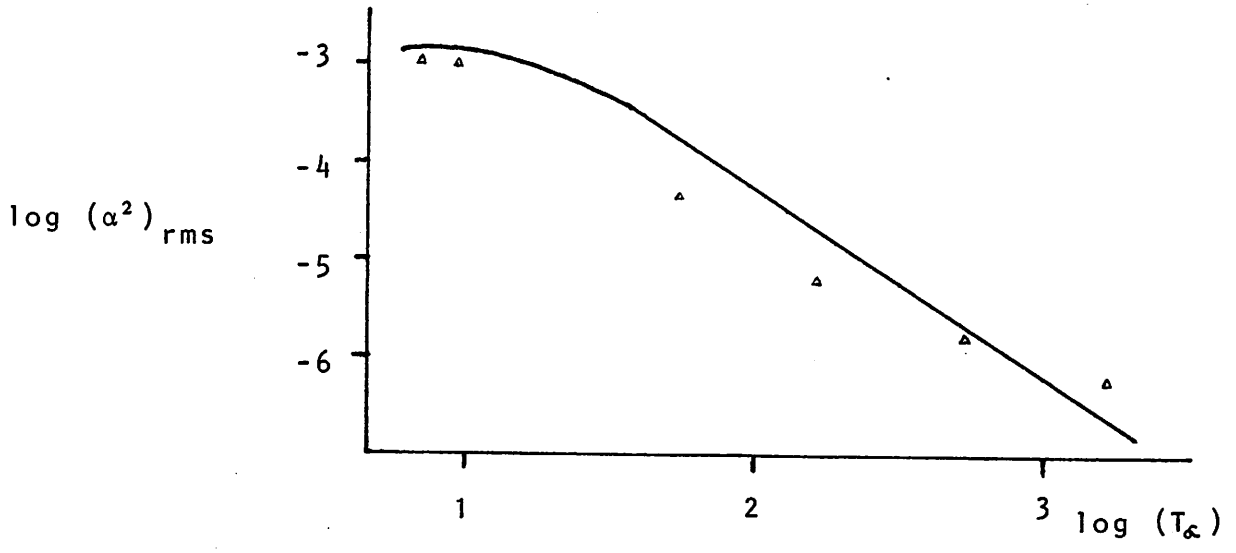

18b. Dispersion vs Libration Period

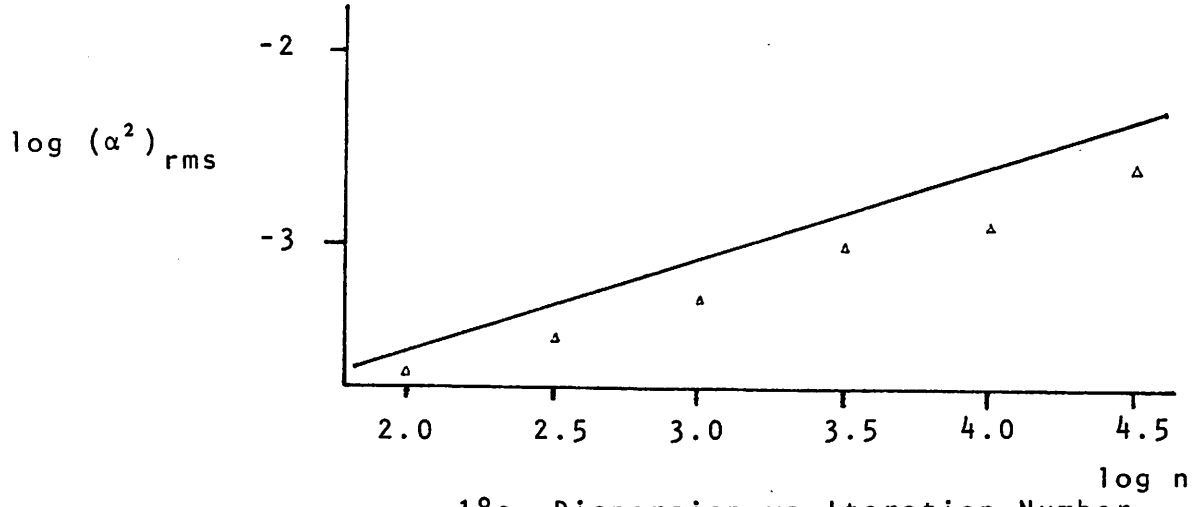

18c. Dispersion vs Iteration Number